Kinetic and Structural Studies on the Catalytic Role of the Aspartic Acid Residue Conserved in Copper Amine Oxidase[†,‡]

Yen-Chen Chiu,[§,||] Toshihide Okajima,*[,§,⊥] Takeshi Murakawa,[§] Mayumi Uchida,[#] Masayasu Taki,[#] Shun Hirota,[¶] Misa Kim,[£,⊥] Hiroshi Yamaguchi,[£] Yoshiaki Kawano,[⊥] Nobuo Kamiya,[⊥,$] Shun'ichi Kuroda,[§] Hideyuki Hayashi,[▽] Yukio Yamamoto,[#] and Katsuyuki Tanizawa*[,§]

Institute of Scientific and Industrial Research, Osaka University, Ibaraki, Osaka 567-0047, Japan, Graduate School of Human and Environmental Studies, Kyoto University, Kyoto, Japan, Kyoto Pharmaceutical University, Yamashina, Kyoto 607-8414, Japan, PRESTO, JST, Kawaguchi, Saitama 332-0012, Japan, School of Science and Technology, Kwansei Gakuin University, Sanda, Hyogo 669-1337, Japan, Institute of Physical and Chemical Research, RIKEN Harima Institute/SPring-8, Mikazuki-cho, Sayo, Hyogo 679-5148, Japan, and Department of Biochemistry, Osaka Medical College, Takatsuki, Osaka 569-8686, Japan

Received December 2, 2005; Revised Manuscript Received February 14, 2006

ABSTRACT: Copper amine oxidase contains a post-translationally generated quinone cofactor, topa quinone (TPQ), which mediates electron transfer from the amine substrate to molecular oxygen. The overall catalytic reaction is divided into the former reductive and the latter oxidative half-reactions based on the redox state of TPQ. In the reductive half-reaction, substrate amine reacts with the C5 carbonyl group of the oxidized TPQ, forming the substrate Schiff base (TPQ_{ssb}), which is then converted to the product Schiff base (TPQ_{psb}). During this step, an invariant Asp residue with an elevated pK_a is presumed to serve as a general base accepting the α proton of the substrate. When Asp298, the putative active-site base in the recombinant enzyme from *Arthrobacter globiformis*, was mutated into Ala, the catalytic efficiency dropped to a level of about 10^6 orders of magnitude smaller than the wild-type (WT) enzyme, consistent with the essentiality of Asp298. Global analysis of the slow UV/vis spectral changes observed during the reductive half-reaction of the D298A mutant with 2-phenylethylamine provided apparent rate constants for the formation and decay of TPQ_{ssb} ($k_{obs} = 4.7$ and 4.8×10^{-4} s^{-1}, respectively), both of which are markedly smaller than those of the WT enzyme determined by rapid-scan stopped-flow analysis ($k_{obs} = 699$ and 411 s^{-1}, respectively). Thus, Asp298 plays important roles not only in the α-proton abstraction from TPQ_{ssb} but also in other steps in the reductive half-reaction. X-ray diffraction analyses of D298A crystals soaked with the substrate for 1 h and 1 week revealed the structures of TPQ_{ssb} and TPQ_{psb}, respectively, as pre-assigned by single-crystal microspectrophotometry. Consistent with the stereospecificity of α-proton abstraction, the *pro-S* α-proton of TPQ_{ssb} to be abstracted is positioned nearly perpendicularly to the plane formed by the Schiff-base imine double bond conjugating with the quinone ring of TPQ, so that the orbitals of σ and π electrons maximally overlap in the conjugate system. More intriguingly, the *pro-S* α proton of the substrate is released stereospecifically even in the reaction catalyzed by the base-lacking D298A mutant. On the basis of these results, we propose that the stereospecificity of α-proton abstraction is primarily determined by the conformation of TPQ_{ssb}, rather than the relative geometry of TPQ and the catalytic base.

Copper amine oxidases (CAOs)[1] catalyze the oxidative deamination of various primary amines and are widely occurring from prokaryotes to eukaryotes (*1*). All CAOs well-characterized thus far are the homodimers of a ∼70−95-kDa subunit, each containing a Cu^{2+} ion and a quinone

[†] This study was supported by Grants-in-Aid for Scientific Research from the Ministry of Education, Culture, Sports, Science, and Technology of Japan (the 21st Century Center of Excellence Program, to K.T.) and from the Japan Society for the Promotion of Science (Category C, number 14560066, to T.O., and Exploratory Research, number 16655070, to Y.Y.).

[‡] The atomic coordinates and structure factors for the substrate-free holo D298A and those soaked with 2-PEA for 1 h and 1 week have been deposited in the Protein Data Bank with the accession codes 2CWT, 2CWU, and 2CWV, respectively.

* To whom correspondence should be addressed. Telephone: +81-6-6879-4292. Fax: +81-6-6879-8460. E-mail: tokajima@sanken.osaka-u.ac.jp (T.O.); tanizawa@sanken.osaka-u.ac.jp (K.T.).

[§] Osaka University.

[||] Present address: Department of Exercise and Health Sciences, National Taiwan College of Physical Education, Shuang-shih Road, Taichung 404, the Republic of China (Taiwan).

[⊥] RIKEN Harima Institute.

[#] Kyoto University.

[¶] Kyoto Pharmaceutical University and JST.

[£] Kwansei Gakuin University.

[$] Present address: Department of Chemistry, Graduate School of Science, Osaka City University, Osaka 558-8585, Japan.

[▽] Osaka Medical College.

[1] Abbreviations: ABTS, 2,2′-azinobis(3-ethylbenzothiazoline-6-sulfonic acid); AGAO, *Arthrobacter globiformis* amine oxidase; CAO, copper amine oxidase; BSAO, bovine serum amine oxidase; ECAO, *Escherichia coli* amine oxidase; HPAO, *Hansenula polymorpha* amine oxidase; 2-PEA, 2-phenylethylamine; PSAO, pee seeding amine oxidase; TPQ, topa quinone; TPQ_{psb}, product Schiff base; TPQ_{ssb}, substrate Schiff base; TPQ_{imq}, TPQ in the iminoquinone form; TPQ_{ox}, TPQ in the oxidized form; TPQ_{red}, TPQ in the reduced form (an aminoresorcinol form); TPQ_{sq}, topa semiquinone.

10.1021/bi052464l CCC: $33.50
Published on Web 03/14/2006

cofactor named topa quinone (TPQ) that is generated post-translationally from a specific tyrosine residue encoded in the polypeptide chain (*2*−*6*). We determined the crystal structure of a recombinant enzyme cloned from a Gram-positive bacterium *Arthrobacter globiformis* (AGAO) at 2.2-Å resolution using the diffraction data obtained at an ambient temperature (*7*) and more recently at 1.8-Å resolution using those obtained at a cryo-temperature (*8*). The crystal structures of CAOs from pea seedling (PSAO) (*9*), *Escherichia coli* (ECAO) (*10*), yeast *Hansenula polymorpha* (HPAO) (*11*), *Pichia pastoris* (lysyl oxidase) (*12*), bovine serum (BSAO) (*13*), and most recently, human vascular membrane (a CAO that was identified as vascular adhesion protein 1 and found to be identical with semicarbazide-sensitive amine oxidase) (*14*) have also been determined; despite rather low sequence similarities, they all have very similar polypeptide folds and active-site structures. The overall catalytic reaction of CAOs proceeds by the ping-pong bi-bi mechanism and consists of the initial reductive and subsequent oxidative half-reactions, involving $2e^-$ reduction of the oxidized cofactor (TPQ_{ox}) by the substrate and reoxidation of the reduced one (TPQ_{red}) by molecular oxygen, respectively.

In the initial half-reaction, the amine substrate reacts with the C5 carbonyl oxygen of TPQ_{ox}, yielding the substrate Schiff base (TPQ_{ssb}) (*15*, *16*), in which the pK_a of the Cα proton of the substrate is expected to be decreased significantly. An invariant Asp residue located close to the TPQ cofactor has been believed to serve as a catalytic base (*17*−*19*), accepting the substrate Cα proton to form the product Schiff base (TPQ_{psb}) with concomitant reduction of the cofactor quinone ring (*15*, *16*). Following hydrolysis of TPQ_{psb} leads to the formation of the first product aldehyde and TPQ_{red} in the aminoresorcinol form (*15*, *16*). The reductive half-reaction proceeds independently of the bound copper ion (*8*, *15*). The latter half-reaction consists of the steps of regenerating TPQ_{ox} from TPQ_{red} and involves the net $2H^+$ and $2e^-$ transfers from TPQ_{red} to dioxygen, during which the copper ion plays an important role by serving as an electron mediator between TPQ_{red} and O_2. This role of copper was initially proposed on the basis of the observation of the temperature-dependent, rapid equilibrium between the Cu^{2+}/TPQ_{red} state and the Cu^{1+}/topa semiquinone (TPQ_{sq}) state, suggesting that the latter state is kinetically competent (*20*, *21*). However, later kinetic studies on the oxidative half-reaction have implicated that the initial $1e^-$ reduction of O_2 occurs directly from the Cu^{2+}/TPQ_{red} couple but not from the Cu^{1+}/TPQ_{sq} couple (*22*). Moreover, our metal-substitution study (*8*) has also suggested that the bound metal ion does not change its redox state but provides a binding site for $1e^-$- and $2e^-$-reduced oxygen species to be efficiently protonated and released as a final product, H_2O_2. Under the turnover conditions, an iminoquinone form of TPQ (TPQ_{imq}) formed during the oxidative half-reaction may react directly with substrate amine to form TPQ_{ssb} (by transimination), while TPQ_{ox} is on the route in the single-turnover reaction (*8*). Model studies have indicated that the transimination is several orders of magnitude faster than the hydrolysis of TPQ_{imq} (*16*).

An Asp residue strictly conserved in the active site of CAOs has been shown to be a key residue participating in the reductive half-reaction, most likely acting as a general base accepting the Cα proton of the substrate in the TPQ_{ssb} intermediate with an elevated pK_a value (*23*). Asp383 of ECAO and Asp319 of HPAO correspond to this conserved Asp, and their essentiality has already been demonstrated by site-specific mutagenesis (*17*, *18*). Further evidence has been presented that the conserved Asp participates in accepting a proton from the protonated substrate amine to facilitate TPQ_{ssb} formation (*24*). Although a structural role in stabilizing a productive conformation of TPQ (*19*) and/or controlling the mobility of the TPQ ring for optimal activity (*18*) has also been proposed for the conserved Asp, further details of its catalytic role remain to be unraveled. In the present study herein reported, we have mutated Asp298, the Asp residue conserved in AGAO, into Ala and analyzed the catalytic properties of the D298A mutant enzyme that showed only a minuscule activity. Important new findings obtained are that (i) the *pro-S* α proton of the substrate is released stereospecifically regardless of the presence of the H^+-accepting Asp298, (ii) the TPQ_{psb} formation including the α-proton abstraction from TPQ_{ssb} is not the rate-limiting step in the reductive half-reaction of AGAO, and furthermore, (iii) X-ray crystal structures of the TPQ_{ssb} and TPQ_{psb} intermediates have been determined for the first time, revealing a conformation of TPQ_{ssb}, which could further define the *pro-S* stereospecificity of α-proton abstraction in the AGAO catalysis (*25*) as an intrinsic structural feature of the catalytic intermediate.

EXPERIMENTAL PROCEDURES

Materials. Stereospecifically deuterium-labeled substrates, (*R*)-[1-^{2}H]- and (*S*)-[1-^{2}H]-2-phenylethylamine (2-PEA), were synthesized as described previously (*25*). Synthetic oligonucleotides were purchased from GENSET OLIGO. All other chemicals were of the highest grade commercially available and were used without further purification. All buffers and culture media for enzyme expression were prepared with ultrapure water obtained from a NANO pureII (Barnstead).

Mutant Preparation. Site-specific mutagenesis for Asp298 was carried out using a QuikChange site-directed mutagenesis kit (STRATAGENE) with a sense primer (5′-AGAACTACTTCGCTACGGGGGAG-TACCTG-3′) and an antisense primer (5′-CAGGTACTCCCCCGTAGCGAAGTAGTTCT-3′) containing mismatching bases (underlined) for the mutated codon and plasmid pEPO-02 (*8*) encoding the wild-type (WT) enzyme as a template. PCR was performed in a thermal cycle reactor (Perkin Elmer, GeneAmp PCR System 2400) with 30 cycles of denaturation at 95 °C for 30 s, annealing at 55 °C for 1 min, and elongation at 68 °C for 10 min. An amplified DNA was treated with *Dpn*I to digest the WT template DNA. After the digest was transformed into *E. coli* DH5α, an expression plasmid for D298A, pEPO-02-D298A, was isolated from a single clone. The DNA sequence of the mutant gene was confirmed with an Applied Biosystems 377 DNA sequencer; no undesired mutation was detected in the entire AGAO gene.

Enzyme Expression and Purification. E. coli CD03, a mutant strain of *E. coli* BL21(DE3) with two catalase genes disrupted (*8*), carrying the expression vector pEPO-02-D298A, was cultivated in a copper-depleted medium, and the D298A mutant enzyme was purified to homogeneity (purity, >99% as judged by SDS−PAGE) in the Cu^{2+}/TPQ-

less apo form as described previously (*4*). The Cu^{2+}/TPQ-containing holo form of D298A was prepared by dialysis of the apoenzyme against 3 L of 50 mM HEPES buffer at pH 6.8 containing 50 μM $CuSO_4$ at 4 °C for 48 h, followed by dialysis against 3 L of 50 mM HEPES buffer at pH 6.8 containing 1 mM ethylenediaminetetraacetic acid at 4 °C for 24 h to remove unbound or weakly bound Cu^{2+} ions. Similarly, the WT enzyme was also purified in the apo form and converted to the holo form. Protein concentrations were spectrophotometrically determined using extinction coefficients at 280 nm of 12.3 and 13.2 for 1% (w/v) solutions of the apo and holo forms, respectively (*4*), and expressed as subunit concentrations unless otherwise stated.

Rate of TPQ Formation. The rate of TPQ formation was determined spectrophotometrically in the reaction mixture containing 0.1 mM apo AGAO subunit (WT and D298A mutant) and 0.5 mM $CuSO_4$ in 50 mM HEPES buffer at pH 6.8. The reaction was performed at 30 °C under atmospheric conditions, and absorption spectra were recorded every 10 s with a photodiode-array spectrophotometer. The observed rate constants (k_{obs}) for TPQ formation were calculated by fitting the absorbance changes at 450 nm (D298A) and 480 nm (WT) plotted against time to a single exponential curve as described previously (*4*, *26*).

Determination of TPQ and Copper Contents. The reactivity of TPQ with phenylhydrazine was analyzed by incubating 5 μM holo AGAO with 20 μM phenylhydrazine prepared freshly in 500 μL of 50 mM HEPES buffer at pH 6.8 and monitoring the absorbance changes at 438 nm. The first-order rate constants for the absorbance changes were obtained by a least-squares exponential fit using Kaleidagraph version 3.0 (Abelbeck Software) on an i386-compatible PC platform. The cofactor content of the holo WT enzyme was determined by titration with phenylhydrazine as described previously (*4*, *8*). As for D298A, the cofactor content could not be determined because of its extremely slow reaction with phenylhydrazine (see the Results). As an alternative way, assuming that the molar absorption coefficient (ϵ_M) of TPQ is the same for the WT and D298A mutant enzymes, an approximate TPQ content was estimated from the absorbance value of TPQ at each λ_{max} after correction for enzyme concentrations. Copper contents were determined with a Shimadzu AA-6400G atomic absorption spectrophotometer equipped with a GFA-6500 graphite furnace atomizer using a commercially available copper solution (100 ppm, Nacalai Tesque) as a standard.

Enzyme Assay. The enzyme activity was assayed spectrophotometrically at 15 or 30 °C as indicated in 100 mM HEPES buffer at pH 6.8 with 40 μM 2-PEA as the substrate, by monitoring H_2O_2 production coupled to the oxidation of 2 mM 2,2′-azinobis(3-ethlybenzthiazoline-6-sulfonic acid) (ABTS) (ϵ_{414} = 24.6 mM^{-1} cm^{-1}) using 10 units/mL of horseradish peroxidase (Wako Pure Chemicals) (*4*). One unit of enzyme is defined as the amount that catalyzes the production of 1 μmol of H_2O_2/min under the assay conditions. Steady-state kinetic parameters were determined on the basis of the ping-pong bi-bi mechanism, by systematically changing the concentration of 2-PEA with an atmospheric O_2 concentration. The kinetic data were fitted to the Michaelis−Menten equation by nonlinear regression using Kaleidagraph version 3.0 (Abelbeck Software).

Resonance Raman Spectroscopy. Resonance Raman scattering was excited at 514.5 nm with an Ar^+ ion laser (Spectra Physics, 2017) and detected with a triple polychromator (JASCO, NR-1800) equipped with a CCD detector (Princeton Instruments). The excitation laser beam power was adjusted to 50 mW at the sample point. Measurements were carried out at room temperature in a spinning cell (3000 rpm). The data accumulation time was 600 s. Raman shifts were calibrated with acetone, and the resolution of the Raman bands was ±1 cm^{-1}.

Stereochemical Analysis of Proton Abstraction. The reaction mixture (total volume of 1 mL) containing 0.014 mM D298A, 0.2 unit/mL of equine liver alcohol dehydrogenase (Sigma), 0.2 mM NADH, 40 μM (*R*)-[1-^{2}H]- or (*S*)-[1-^{2}H]-2-PEA, and 100 mM HEPES buffer at pH 6.8 was incubated at 30 °C for a total of 8 h. To keep the spontaneous oxidation of NADH as minimum as possible, 0.2 mM NADH and 40 μM ^{2}H-labeled 2-PEA were supplemented 4 times at every 2 h during the reaction. In this system, phenylacetaldehyde (the oxidation product from 2-PEA) is immediately converted to the corresponding alcohol (2-phenylethyl alcohol) by the coupled reaction with alcohol dehydrogenase. The completed reaction mixture was extracted with 0.5 mL of ethyl acetate. An aliquot (∼2−4 μL) of the extracted solution was applied onto GC−MS equipment (Shimadzu GC-17A, GCMS-QP5050A) to measure the mass of the alcohol. The instrumental conditions were as reported previously (*25*).

Spectrophotometric Measurements. Spectral changes occurring during the reductive half-reaction were monitored at 15 °C using an Applied Photophysics SX.17MV rapid-scan stopped-flow spectrometer with all lines and reservoir cylinders maintained under fully anaerobic conditions. Typically, equal volumes (about 30 μL each) of the enzyme solution (0.2 mM subunit for both the WT and D298A mutant in 50 mM HEPES buffer at pH 6.8) and the substrate solution (8 mM 2-PEA) were mixed in a mixing cell (volume of 20 μL) triggered with an N_2-gas piston; the mixing dead time was generally 2.3 ms at an N_2-gas pressure of 500 kPa. UV/vis absorption spectra were recorded every 2.5 ms in a wavelength region of 250−800 nm. When the slower process of the reductive half-reaction was monitored by D298A, the enzyme and substrate solutions were mixed manually using gastight syringes (final concentration, 0.14 mM subunit and 4 mM 2-PEA; final volume of 0.2 mL) in a quartz cuvette with a screw cap and the spectra were recorded at 15 °C using an Agilent 8453 photodiode-array spectrophotometer equipped with an Agilent 89090A temperature-control accessory. To avoid spectral changes associated with the oxidative half-reaction, both enzyme and substrate solutions were kept in a vacuum-type glovebox (Iuchi, SGV-65V) filled with 99.999% Ar gas for at least 6 h before the stopped-flow and manual mixing measurements and handled using gastight syringes. Spectral data were analyzed by a Pro-Kineticist II (Applied Photophysics) software to obtain spectra of the reaction intermediates and to calculate the rate constants for each reaction step.

pH Profile. To avoid inconsistencies from changing buffer components for the measured pH range from 6.0 to 10.0, buffers were prepared by mixing equal volumes of 0.2 M CHES, MOPS, and MES and titrating to the desired pH values with 1 M NaOH. The ionic strengths of buffers were maintained at 0.2 by the addition of an appropriate amount

of Na_2SO_4 (*27*). For the measurement of the pH profile, the ABTS method could not be used in the acidic region because horseradish peroxidase used as a coupling enzyme was proven to be inactive below pH 6.4. Therefore, in the case of WT AGAO, a Clark-type oxygen electrode (Toko Chemical Laboratories) was used to measure the enzyme activity in terms of monitoring the rate of oxygen consumption. The reaction was initiated by adding 1.0 nM WT enzyme into the buffer at various pH (final volume of 1 mL), containing varied concentrations (2−20 μM) of 2-PEA. However, this assay method was not applicable to D298A because of the necessity of using a fairly large amount of the mutant enzyme with a very low activity. Thus, the coupling method with alcohol dehydrogenase described above for the stereochemical analysis was used to measure the activity of D298A in a broad pH range. The reaction mixture contained an appropriate amount of D298A, 0.2 mM NADH ($\epsilon_{340} = 6220$ M^{-1} cm^{-1}), 0.2 unit/mL of alcohol dehydrogenase, and various concentrations (2.5−50 μM) of 2-PEA in the buffer at various pH (final volume of 0.4 mL), and the decrease in absorbance at 340 nm because of the NADH consumption was measured at 30 °C. The k_{cat} and k_{cat}/K_m values obtained were plotted against pH and analyzed by fitting the data to one of the following equations, where y represents the value of k_{cat} or k_{cat}/K_m at particular pH, C is the pH-independent maximum value of the parameter [$(k_{cat})_{max}$ or $(k_{cat}/K_m)_{max}$], and K_{a_1} and K_{a_2} are acid dissociation constants associated with ionizable groups on the acid and alkaline limbs, respectively, of pH profiles (*28*).

$$\log y = \log\left(\frac{C}{1 + [H^+]/K_{a_1} + K_{a_2}/[H^+]}\right) \quad (1)$$

$$\log y = \log\left(\frac{C}{1 + [H^+]/K_{a_1}}\right) \quad (2)$$

$$\log y = \log\left(\frac{C}{1 + K_{a_2}/[H^+]}\right) \quad (3)$$

Crystallization and Single-Crystal Microspectrophotometry. The holo D298A was crystallized by the microdialysis method as described previously (*8*). The enzyme solution (10 mg/mL) was placed in a 50-μL button and dialyzed at 16 °C against 1.05 M potassium−sodium tartrate in 25 mM HEPES buffer at pH 6.8. Single crystals with approximate dimensions of 0.2 × 0.4 × 0.1 mm grew in about 2 weeks, and then the dialysis buttons were transferred into the new reservoir solution supplemented with 45% (v/v) glycerol as a cryoprotectant. For determination of the crystal structures of the TPQ_{ssb} and TPQ_{psb} intermediates generated in the active site, the holo D298A crystals were further soaked at 16 °C for 1 h to 1 week in the new reservoir solution containing 45% (v/v) glycerol and 3 mM 2-PEA. Before exposure to X-ray, the crystals were analyzed by single-crystal microspectrophotometry at 100 K. The microspectrophotometer system consisted of a deuterium tungsten halogen light (Ocean Optics, DT-MINI), Cassegrainian mirrors (Bunkoh-Keiki Co. Ltd.), an optical fiber, and a linear CCD-array spectrometer (Ocean Optics, SD2000). Absorption spectra were recorded in the wavelength region of 178−879 nm and corrected for the air blank baseline and dark reference.

Data Collection and Refinement. X-ray diffraction data were collected at 100 K with the synchrotron X-radiation ($\lambda = 1.0$ Å) using a Quantum 4 detector (ADSC) in the station BL18B at Photon Factory (Tsukuba, Japan) for free holo D298A crystals and at 100 K with the synchrotron X-radiation ($\lambda = 0.9$ Å) using a PX210 detector (Oxford) in the station BL44XU at SPring-8 (Hyogo, Japan) for substrate-soaked D298A crystals. The diffraction data collected for these crystals were processed and scaled using MOSFLM (*29*) and SCALA (*30*), respectively. These crystals were found to belong to the space group *I2* as reported for the WT AGAO crystals at a cryo temperature (*8*). The details and statistics of data collection are summarized in Table 1. The program used for refinements, calculation of electron-density maps, and assignment of solvent molecules was CNS version 1.1 (*31*). Manual rebuilding was performed using an xfit module in the XtalView software package (*32*). The WT structure (PDB code 1IU7) without solvent molecules was used as an initial model, with TPQ382 being replaced with an unmodified Tyr residue. After subjecting to the rigid-body refinement, initial structures of the free and substrate-soaked holo D298A crystals were further refined through simulated annealing from 3000 K and several cycles of *B*-factor and positional refinements. In the modeling stage, the residues at the mutated sites were replaced with an Ala residue based on the $F_o - F_c$ and $2F_o - F_c$ electron-density maps. The models of the substrate Schiff-base complexes (TPQ_{ssb} and TPQ_{psb}) were built using Insight II (Accelrys, CA), and then topology and parameter files for refinement used for CNS were generated with XPLO2D in the X-UTIL package (*33*). Residues at position 382 of the holo D298A and the two substrate-soaked structures were replaced by the oxidized form of TPQ, TPQ_{ssb}, and TPQ_{psb}, respectively, on the basis of the $2F_o - F_c$, $F_o - F_c$, and omit maps. Metal ions were assigned on the basis of the highest peaks in the respective $2F_o - F_c$ maps; water molecules and residues in the active-site region were carefully examined using $2F_o - F_c$, $F_o - F_c$, and omit maps. These models were refined through further several cycles of *B*-factor and positional refinements after introducing solvent molecules. The details and statistics of crystallographic refinement are also summarized in Table 1.

RESULTS

TPQ Generation in the D298A Mutant. Several fundamental properties of the D298A mutant enzyme purified in the apo form and then dialyzed against $CuSO_4$-containing buffer for cofactor generation are summarized in Table 2, together with those of the WT enzyme for a comparison. The copper content in D298A was estimated to be about 0.9 mol/mol of subunit, which is similar to the content in the WT enzyme, indicating that the copper-binding ability was minimally affected by the mutation of Asp298 to Ala. An absorption spectrum of D298A (Figure 1A) also suggested that the TPQ cofactor was correctly generated in D298A, as in the WT enzyme. However, an attempt to determine the TPQ content by spectrophotometric titration with phenylhydrazine (*34*) was unsuccessful because of the extremely slow reaction of the D298A mutant with phenylhydrazine ($k_{obs}^{WT}/k_{obs}^{D298A} = \sim 170$, see Table 2), as reported for the analogous catalytic base mutants of HPAO (*18*) and ECAO (*19*). Therefore, assuming that the molar absorption

Table 1: Statistics of Data Collection and Crystallographic Refinement

	substrate-free D298A	D298A/2-PEA(*h*)	D298A/2-PEA(*w*)
data collection			
temperature (K)	100	100	100
wavelength (Å)	1.00	1.00	1.00
space group	*I*2	*I*2	*I*2
unit cell dimensions			
a, *b*, *c* (Å)	157.67, 63.80, 184.45	157.84, 62.73, 183.89	157.70, 62.85, 184.13
β (deg)	112.40	112.31	112.43
number of observations	521 900	526 624	521 425
number of unique reflections	144 512	140 478	142 534
multiplicity	3.6	3.7	3.7
$d_{max} - d_{min}$ (Å)	30.0−1.82	52.7−1.85	52.0−1.85
overall completeness (%)	99.7	98.9	100
overall R_{merge} (%)[a]	5.8	8.7	13.4
refinements statistics			
$d_{max} - d_{min}$ (Å)	30−1.82	40−1.85	40−1.85
residues in the core ϕ, φ region (%)	88.5	89.4	88.5
number of solvent atom	838	1229	1080
rms deviation from ideal values			
bond lengths (Å)	0.005	0.005	0.005
bond angles (deg)	1.38	1.38	1.37
residual *R* (%)[b]	19.1	17.7	20.2
free residual *R* (%)[c]	20.1	20.1	23.2

[a] $R_{merge} = \sum_h\sum_i |I_{h,i} - \langle I_h\rangle|/\sum_h\sum_i I_{h,i}$, where $I_{h,i}$ is the intensity value of the *i*th measurement of *h* and $\langle I_h\rangle$ is the corresponding mean value of I_h for all *i* measurements. [b] $R = \sum||F_o| - |F_c||/\sum|F_o|$. [c] Free residual *R* is an *R* factor of the CNS refinement evaluated for 5% of the reflections that were excluded from the refinement.

Table 2: Characteristics of the WT and D298A Mutant of AGAO

						steady-state kinetic parameters		
enzyme	rate of TPQ biogenesis (s^{-1})	reaction rate with phenylhydrazine (s^{-1})	specific activity (unit/mg)	copper content (mol/subunit)	TPQ content (mol/subunit)	K_m for 2-PEA (μM)	k_{cat} (s^{-1})	k_{cat}/K_m (μM^{-1} s^{-1})
WT	0.53	14	47	0.89	0.63	2.5 ± 0.025	76 ± 0.76	30
D298A	0.20	0.081	0.000 16	0.90	0.61	2.1 ± 0.8	(2.1 ± 0.2) × 10^{-4}	0.000 10

coefficient of TPQ is the same for both of the WT and mutant enzymes ($\epsilon_M^{TPQ(WT)} = \sim 1800$ M^{-1} cm^{-1}) (*35*), the TPQ content in D298A was estimated from the absorbance value at 460 nm (λ_{max} of TPQ in D298A, see below). An approximate TPQ content in D298A thus estimated was 0.61 mol/mol of subunit, which was comparable to the content in the WT enzyme determined by titration with phenylhydrazine (Table 2). Semiquantitative detection of quinone groups with the alkaline nitroblue tetrazolium/glycinate reagent developed for quinone staining (*36*) also revealed no obvious difference in the TPQ contents of D298A and WT AGAO (data not shown). Thus, Asp298 is not directly involved in the copper-dependent self-processing generation of TPQ, although the rate of TPQ generation is reduced to about 40% of the WT by the mutation (Table 2), the reason for which remains unsettled.

Absorption and Resonance Raman Spectra. We noted that the D298A solution was colored yellowish brown after dialysis against the TPQ-generating buffer containing $CuSO_4$. Indeed, a UV/vis absorption spectrum of holo D298A has revealed that λ_{max} of TPQ (around 460 nm) is blue-shifted by about 26 nm as compared with the WT TPQ, which is colored pink with λ_{max} at 486 nm (Figure 1A). A similar blue shift of TPQ absorption has been reported for the equivalent holo D383A mutant of ECAO (36 nm blue shift) (*19*), indicating that the TPQ ring π electrons are more localized in the mutant enzyme lacking the nearby Asp residue than in the WT enzyme.

Resonance Raman spectra of the holo D298A and WT AGAO have also revealed that the Raman band at a wavenumber of 1685 cm^{-1} in the WT spectrum, which had been assigned to the C═O stretch of the C5 carbonyl group of TPQ (*37*), is upshifted by 9 cm^{-1} in the D298A spectrum (Figure 1B). This indicates that the C5═O group of TPQ has a greater double-bond character in D298A than in the WT enzyme. In contrast, the band at 1579 cm^{-1}, assigned to the C═O stretch of the C2 carbonyl group of TPQ (*37*), is downshifted by 6 cm^{-1} in D298A, which indicates that the C2═O group of TPQ has a more single-bond character in D298A than in the WT enzyme. Other vibrational modes, particularly in the lower energy field (∼1100−1500 cm^{-1}), correspond well with each other in peak frequencies and intensities. In combination with the 26 nm blue shift of λ_{max} in the UV/vis absorption spectrum, these results demonstrate that the TPQ ring π electrons are more uniformly delocalized in the WT enzyme than in the D298A mutant, in which electrons on the C5═O carbonyl group are less conjugating with the ring π-electron system. Thus, although there is no direct interaction between TPQ and Asp298 in the active-site structure of WT AGAO (*8*) (see Figure 6C), the electronic properties of TPQ are significantly affected by the presence of the presumed catalytic base, Asp298. In the HEPES buffer at pH 6.8 used for spectral measurements, the side-chain carboxyl group of Asp298 would be dominantly protonated because of its elevated pK_a value (∼7.5, see below) and thereby could form a weak hydrogen bond

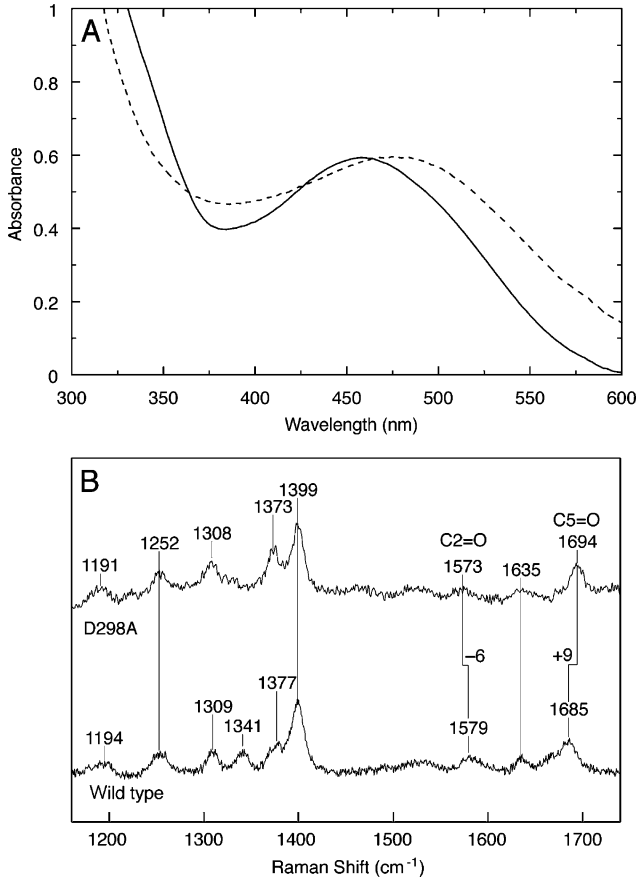

FIGURE 1: UV/vis absorption and resonance Raman spectra. (A) Absorption spectra of the WT (- - -) and D298A mutant (—) of AGAO were measured in 50 mM HEPES buffer at pH 6.8 both at a subunit concentration of 0.28 mM. (B) Resonance Raman spectra of the D298A (upper) and WT (lower) AGAO were measured at room temperature in 50 mM HEPES at pH 6.8 both at a subunit concentration of 0.15 mM. The ordinate scales are normalized with the intensity of the 1399 cm^{-1} band of the WT AGAO, and the spectra are offset for clarity. Frequency shifts calibrated with acetone and toluene standards are indicated above the peaks. See the Experimental Procedures for instrumental conditions.

with the C5═O group in the WT enzyme (3.5 Å) (*8*), leading to partial electron withdrawal from the C5═O double bond. Another possible cause for the blue shift of λ_{max} of TPQ is that there is a water molecule (Wat1) hydrogen-bonding to the C4−O^- group of TPQ in D298A, which is absent in the WT enzyme as described later for X-ray crystal structures (Figure 6C). This hydrogen bond would increase the single bond character of the C2═O group that is conjugating with the C4−O^- group (*38*). It is also likely that the absence of Asp298 and the presence of Wat1 both contribute simultaneously to the blue shift of λ_{max} of TPQ.

Catalytic Properties. The D298A mutant enzyme exhibited almost no enzymatic activity when measured under the standard assay conditions. However, careful measurements using a very large amount (>1 mg) of the purified D298A have revealed that it does possess an extremely low activity, estimated to be $\sim10^5$−10^6 orders of magnitude smaller than the WT activity (Table 2). This minuscule activity of D298A is due to neither experimental errors nor the contamination of the WT enzyme, because the purified D298A mutant showed completely no activity before activation in the TPQ-generating buffer. This result contrasts with those of previous mutagenesis studies (*17*−*19*, *24*), in which the replacement of the conserved Asp residue with other amino acid residues (except for Glu) resulted in the complete disappearance of catalytic activities, even though TPQ was normally generated. Presumably, such a low activity as found in the D298A mutant of AGAO is detectable only by using a very large amount of the purified enzyme. Steady-state kinetic parameters determined for D298A indicated that the K_m value for 2-PEA is comparable with that of the WT enzyme, while the k_{cat} values determined at 30 °C are different by $\sim10^5$-folds between the WT and D298A mutant (Table 2), revealing that the decrease of the catalytic activity of D298A is derived mostly from the marked drop in the k_{cat} value.

Effect of pH on Steady-State Kinetic Parameters. Steady-state kinetic parameters of the WT and D298A mutant enzymes were determined under various pH conditions, and the values of log(k_{cat}) and log(k_{cat}/K_m) for 2-PEA were plotted against pH (Figure 2). The plot of log(k_{cat}/K_m) for 2-PEA versus pH of the WT enzyme was bell-shaped, giving pK_a values of 7.5 ± 0.2 for a group on the acid limb and 8.7 ± 0.2 for a group on the alkaline limb by fitting the data to eq 1 (Figure 2A). The ionizing group on the acid limb must be deprotonated, and the ionizing group on the alkaline limb must be protonated in the free state before catalysis. On the basis of equivalent assignments made by Farnum et al. on BSAO (*23*), Hevel et al. on HPAO (*39*), and Murray et al. on ECAO (*19*), the former group with a pK_a of 7.5 is assigned to the side-chain carboxyl group of Asp298, which must be deprotonated for the reaction to occur. The latter ionizing group with a pK_a of 8.7 may be assigned to the amino group of the substrate, which interacts with the enzyme in its protonated form. For the D298A mutant, only a single ionizable group was observed on the acid limb with a pK_a of 6.8 ± 0.1 (Figure 2B), which is too low to be attributed to a primary amino group [pK_a reported for 2-PEA = 9.78 (*40*)]. Although the group with this low pK_a value remains to be assigned, the similar pH dependence has been observed in the reaction of tranylcypromine with an active-site mutant of ECAO, in which the pK_a was not determined but estimated to be less than 6 (*24*). The pH-independent values of $(k_{cat}/K_m)_{max}$ were estimated to be (5.5 ± 1.5) × 10^7 and 57.1 ± 5.8 M^{-1} s^{-1} for WT and D298A, respectively, again showing that the mutation of Asp298 to Ala resulted in an about 10^6-fold decrease of the catalytic efficiency.

The plot of log(k_{cat}) versus pH of the WT enzyme was also bell-shaped, giving pK_a values of 6.5 ± 0.1 and 8.8 ± 0.1 (Figure 2C). Thus, the pK_a of the carboxyl group of Asp298 decreases by about 1 pH unit in the enzyme/substrate complex, and it must be ionized for the subsequent reaction to occur, most likely for accepting the α-H^+ from the TPQ_{ssb} intermediate. The curve of log(k_{cat}) versus pH plot of the D298A mutant declined in the region above pH 8.5 (Figure 2D), giving an apparent pK_a of 9.9 ± 0.2. This group as well as the high pK_a group (8.8) in the WT enzyme should be protonated in the enzyme/substrate complex, but their assignments warrant further studies.

Stereospecificity of α-Proton Abstraction. We have recently reported that the *pro-S* Cα proton of the amine substrate is released stereospecifically during the reaction catalyzed by WT AGAO (*25*). To investigate whether the stereospecificity for α-H^+ release is associated with the presence of the putative H^+ acceptor (Asp298), we have determined the stereospecificity of the α-H^+ abstraction by

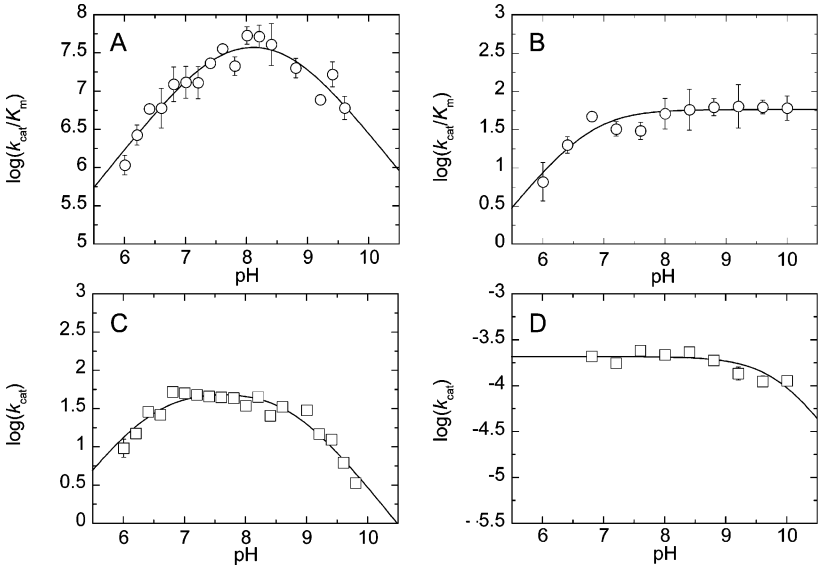

FIGURE 2: pH dependencies of steady-state kinetic parameters. The k_{cat}/K_m values for 2-PEA of the WT (A) and D298A mutant (B) and the k_{cat} values of the WT (C) and D298A mutant (D) were plotted against pH. The units of k_{cat}/K_m and k_{cat} were M^{-1} s^{-1} and s^{-1}, respectively. Curves are the least-squares best fit to eq 1 for the data of the WT enzyme and eq 2 (B) or eq 3 (D) for the data of the D298A mutant.

Table 3: Oxidation of Deuterium-Labeled Chiral Amines by the D298A Mutant of AGAO

		relative peak intensity at *m*/*z*					
configuration of starting 2-PEA	substrate/product	120	121	122	123	124	major component (%)[a]
unlabeled	amine	0.118	1.000[b]	0.098			
	alcohol		0.006	1.000[b]	0.093		
(*R*)-[1-^{2}H]	amine		0.101	1.000[b]	0.125		R-CHDNH$_2$ (>97)
	alcohol			0.012	1.000[b]	0.087	R-CHDOH (>99)
(*S*)-[1-^{2}H]	amine		0.085	1.000[b]	0.110		R-CHDNH$_2$ (>99)
	alcohol		0.007	1.000[b]	0.094		R-CH$_2$OH (>99)

[a] Percent contents of the major component shown in parentheses were calculated from the mass number of the molecular ion peak and the peak intensity, which was rectified with the concomitant M − 1 and M + 1 peaks. R, $C_6H_5CH_2$. [b] Molecular ion peak, M^+.

the D298A mutant using stereospecifically deuterium-labeled substrates, (*R*)-[1-^{2}H]- and (*S*)-[1-^{2}H]-2-PEA. Because the product aldehyde may lose the aldehyde hydrogen (^{1}H or ^{2}H) by auto-oxidation to the corresponding carboxylic acid during a very long period (8 h) needed for the reaction of D298A, possessing only a very low activity, the aldehyde produced was simultaneously converted to the corresponding stable alcohol by the coupled reaction with alcohol dehydrogenase in the presence of NADH. The alcohol was extracted with ethyl acetate, and an aliquot (5−10 μL) of the extract was directly analyzed by GC−MS. The amounts of the deuterium-labeled amines and alcohols were rectified on the basis of the relative intensities of the concomitant M − 1 and M + 1 peaks observed for the nonlabeled amines and alcohols. As summarized in Table 3, both of the alcohols (2-phenylethyl alcohol) obtained in the oxidation of nonlabeled 2-PEA and (*S*)-[1-^{2}H]-2-PEA had a molecular ion peak at 122 Da in the mass spectrum, indicating the loss of the deuterium label during the oxidative deamination of (*S*)-[1-^{2}H]-2-PEA by D298A. On the other hand, when (*R*)-[1-^{2}H]-2-PEA was used, the alcohol had a mass of 123 Da, indicating retention of the deuterium label. The stereoselectivity was calculated to be >99% from the mass spectra of the alcohols obtained from both [^{2}H]-labeled substrates (Table 3). Therefore, it is concluded that the oxidation of 2-PEA by the D298A mutant proceeds in a strictly stereospecific manner, exclusively releasing the *pro-S* hydrogen at the Cα position of substrate amine, as determined for the WT AGAO (*25*). Thus, the stereospecificity for α-H^+ abstraction is completely preserved, regardless of the presence of the H^+-accepting base, Asp298.

Spectral Changes Observed during the Reductive Half-Reaction. To identify the reaction step(s) accounting for the markedly decreased catalytic activity of the D298A mutant, UV/vis spectral changes initiated by the addition of a substrate have been measured under the single-turnover (anaerobic) conditions. Such spectral changes are expected to provide a convenient clue to identifying TPQ-related intermediates formed during the reductive half-reaction of CAOs (*41*, *42*). A rapid-scan stopped-flow spectrometer was used to monitor the initial fast reactions of the D298A mutant and WT enzymes, whereas a conventional spectrometer was used to follow the subsequent slow phase of the D298A reaction started by manual mixing. All measurements were done at 15 °C, so that kinetic constants for both very rapid and extremely slow reactions of WT and D298A, respectively, could be directly compared.

Upon anaerobic mixing of the WT enzyme with excess substrate (2-PEA), the 486-nm absorption band of TPQ_{ox} disappeared within the dead time (2.3 ms) of the stopped-flow instrument (Figure 3A). At nearly the same time, an absorption peak at 316 nm and a shoulder band around 410 nm appeared and then decayed concomitantly with the emergence of new peaks at 365, 438, and 465 nm (inset in Figure 3A), which were assigned to TPQ_{sq} (*8*, *43*). No isosbestic points were observed in the initial five spectra

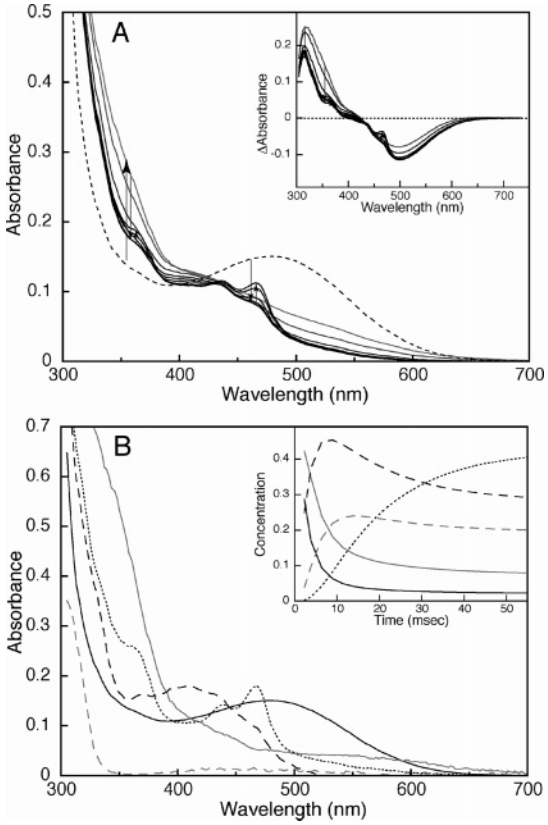

FIGURE 3: Rapid-scan stopped-flow measurements of spectral changes during the reductive half-reaction of WT AGAO. (A) UV/vis absorption spectra were recorded after mixing the WT enzyme (0.1 mM subunit) with 0.5 mM 2-PEA in 50 mM HEPES buffer at pH 6.8 and 15 °C under anaerobic conditions, and the spectra obtained at 2.3, 3.8, 6.4, 9.0, 11, 17, 32, and 63 ms (darker spectra represent later times) are shown. The dashed line represents the initial spectrum of TPQ_{ox}. Arrows indicate the direction of spectral change. (Inset) Difference spectra obtained by the subtraction of the initial TPQ_{ox} spectrum. (B) Deconvoluted absorption spectra obtained by global analysis are shown for TPQ_{ox} (black solid line), TPQ_{ssb} (gray solid line), TPQ_{psb} (black dashed line), TPQ_{red} (gray dashed line), and TPQ_{sq} (black dotted line). (Inset) Time course of concentration changes of each intermediate.

Scheme 1: Reaction Sequence of Reductive Half-Reaction for Global Analysis

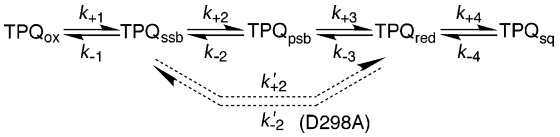

(within 11 ms) but were found at 382 and 429 nm in the four spectra thereafter, suggesting that at least two intermediates are involved in the later phase of the reductive half-reaction. According to the well-accepted mechanism of the reductive half-reaction, TPQ_{ox}, TPQ_{ssb}, TPQ_{psb}, TPQ_{red}, and TPQ_{sq} should be formed in this order and TPQ_{sq} is the final species under the anaerobic conditions (*20*). The multiwavelength data of spectral changes acquired were therefore fit to the four-step model (Scheme 1) by global analysis, where the absorption spectrum of the apo AGAO was used as that of TPQ_{red}, assuming that TPQ_{red} exhibits no absorption above 300 nm (*38*). Also, the absorption spectra of TPQ_{ox} and TPQ_{red} were fixed in the data fitting, while the spectra of other species and rate constants at all steps were varied. Shown in Figure 3B are the deconvoluted UV/vis absorption spectra of TPQ_{ox}, TPQ_{ssb}, TPQ_{psb}, TPQ_{red}, and TPQ_{sq}; the inset shows the time courses of concentration changes of these intermediates. The absorption spectrum obtained for TPQ_{ssb} with a strong shoulder band around 350 nm and a broad and weak one above 400 nm resembles that of a model compound in a nonpolar (CH_2Cl_2) or polar (CH_3CN) aprotic solvent (*16*). Moreover, the spectrum obtained for TPQ_{psb} with a broad peak at 408 nm differs considerably from that of a neutral form of a model compound with a λ_{max} at 368 nm in acetonitrile but resembles that of a monoprotonated form with a λ_{max} at 406 nm (see intermediate G in Scheme 2) (*16*). The calculated spectrum for TPQ_{sq} with absorption peaks at 360, 438, and 467 nm agrees well with those obtained experimentally by anaerobic reduction of AGAO with the substrate (*8*, *43*). Pre-steady-state kinetic constants estimated from the most converged solution in the global analysis (inset in Figure 3B) are summarized in Table 4, together with the steady-state k_{cat} value of the overall reaction determined at 15 °C for a comparison. The k_{+4} value is the smallest among the four rate constants in the forward direction, showing that this step ($TPQ_{red} \rightarrow TPQ_{sq}$) is rate-limiting in the single-turnover (anaerobic) reductive half-reaction of AGAO. Furthermore, it is noteworthy that the rate of the TPQ_{psb} hydrolysis step (k_{+3}; $TPQ_{psb} \rightarrow TPQ_{red}$) is less than half that of the proton abstraction step (k_{+2}; $TPQ_{ssb} \rightarrow TPQ_{psb}$), showing that the hydrolysis of TPQ_{psb} is second rate-limiting in the reductive half-reaction of AGAO.

An anaerobic reaction of the D298A mutant with 2-PEA also resulted in the spectral changes of TPQ, which consisted of the initial relatively fast and subsequent slow phases. In the initial fast phase monitored by stopped-flow spectroscopy, the TPQ-derived 460-nm absorption band decreased slightly and, concomitantly, a new band at 310 nm appeared within 750 ms (inset in Figure 4A). These spectra intersected at about 400 and 540 nm, suggesting that TPQ_{ox} is converted into a single species in this fast phase. The species that formed first is most likely assigned to TPQ_{ssb}, assuming that the reaction pathway of the D298 mutant is essentially identical with that of the WT enzyme. Hence, the multi-wavelength data acquired were fit by global analysis only to the initial step of $TPQ_{ox} \rightarrow TPQ_{ssb}$ (Scheme 1), where the absorption spectrum of D298A TPQ_{ox} was fixed as a starting state and that of TPQ_{ssb} and the rate constants were set variable. The calculated UV/vis spectrum of TPQ_{ssb} (Figure 4C) has a weak shoulder band in the 310−340 nm region and a broad peak at about 450 nm. This spectrum differs considerably from that of TPQ_{ssb} formed in the WT enzyme (Figure 3B) but is similar to that of a model compound in a polar protic solvent (CH_3OH) (*16*). On the basis of the studies using model compounds (*16*), TPQ_{ssb} with a λ_{max} at around 350 nm in the WT enzyme and that with a λ_{max} at around 450 nm in D298A may be assigned to the zwitter ionic and anionic structures, respectively, and an about 100-nm red shift in the latter is presumably due to the resonance delocalization of the negative charge. The rate constant, k_{+1}, calculated from the time courses of the concentration changes (Figure 4D) is also listed in Table 4. Although the initial phase completes within 1 s even with the D298A mutant, the k_{+1} value is about 150-folds smaller than that of the WT enzyme, indicating that Asp298 participates also in the TPQ_{ssb} formation (see the Discussion).

Scheme 2: Detailed Mechanism of Reductive Half-Reaction

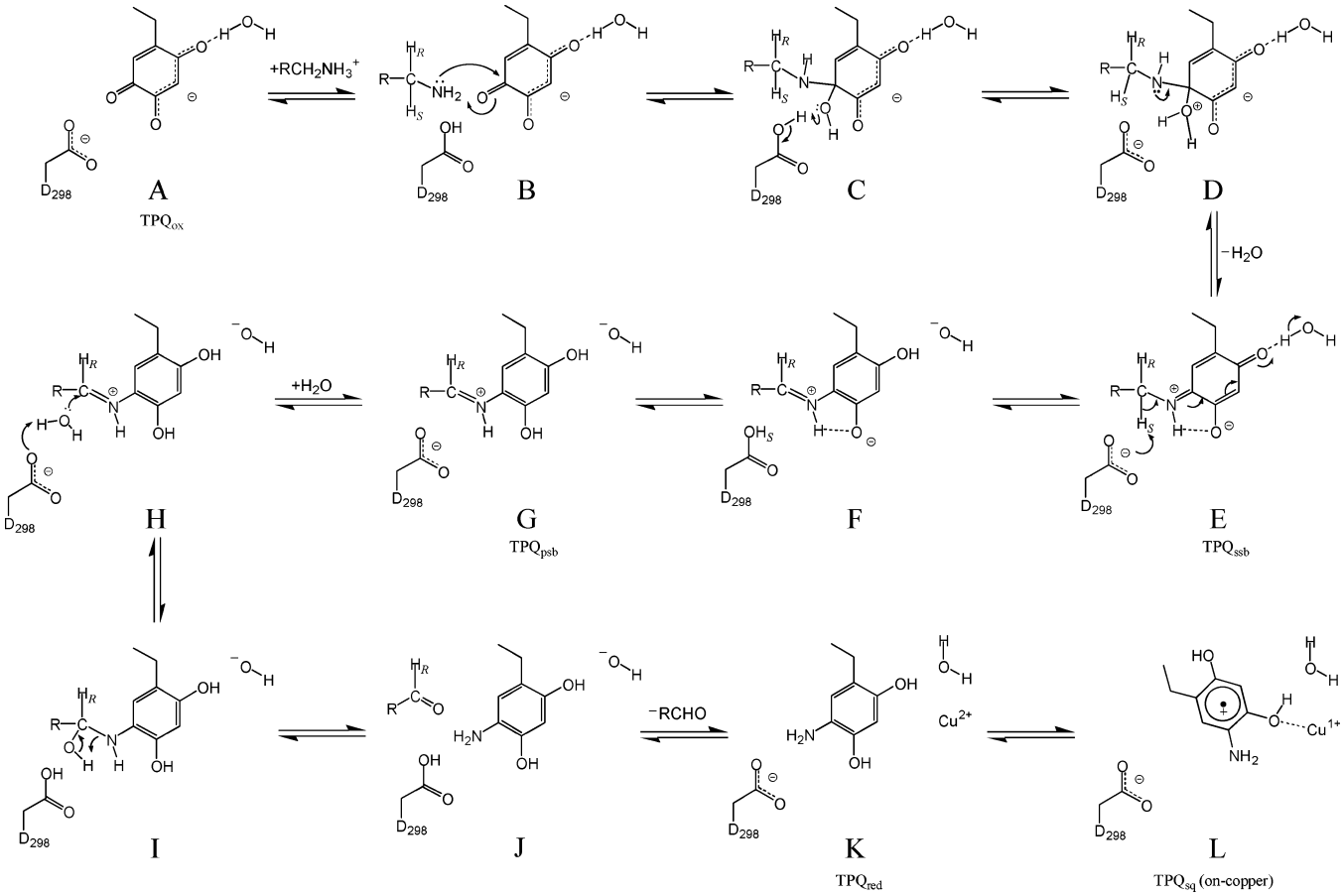

Table 4: Kinetic Constants of Each Step of the Reductive Half-Reaction and Overall Reaction Determined at 15 °C

enzyme	k_{+1} (s^{-1})	k_{+2} (s^{-1})	$k_{+2'}$ (s^{-1})	k_{+3} (s^{-1})	k_{+4} (s^{-1})	k_{-4} (s^{-1})	k_{cat} (s^{-1})
WT	699 ± 75	411 ± 6		197 ± 18	93 ± 120	43 ± 28	44
D298A	4.7 ± 0.02		(4.8 ± 0.0004) × 10^{-4}		(1.4 ± 0.0001) × 10^{-2}	(5 ± 0.00004) × 10^{-2}	1.2 × 10^{-4}

The subsequent slow phase of the D298A reaction was started by manual mixing and monitored with an ordinary spectrometer (Figure 4B). At an initial point of data acquisition that usually took several seconds after starting the reaction by manual mixing, most parts of TPQ_{ox} were already converted to TPQ_{ssb}, consistent with the rate constant obtained by a stopped-flow measurement (k_{+1} = 4.7 s^{-1}, Table 4). However, the following spectral changes were extremely slow, taking several hours, and appeared to involve only two detectable species. Because TPQ_{red} should be invisible in the region above 300 nm, it is suggested that the hydrolysis step ($TPQ_{psb} \rightarrow TPQ_{red}$) is relatively fast as compared with the very slow steps of $TPQ_{ssb} \rightarrow TPQ_{psb}$ and $TPQ_{red} \rightarrow TPQ_{sq}$, and therefore, TPQ_{psb} does not accumulate during the reaction. Hence, the multiwavelength data of spectral changes observed during the slow phase of the D298A reaction were approximated to the three-step model without TPQ_{psb} (Scheme 1; $TPQ_{ssb} \rightarrow TPQ_{red}$, $k_{+2'}$) and fit to this model by global analysis, where the spectra of TPQ_{ssb} and TPQ_{red} were fixed and other parameters were set variable. The resultant absorption spectrum of TPQ_{sq} and time courses of the concentration changes of TPQ_{ssb}, TPQ_{red}, and TPQ_{sq}, all of which converged nicely in the calculation, are shown in parts C and D of Figure 4, and the rate constants ($k_{+2'}$ and k_{+4}) estimated thereof are listed in Table 4. The calculated spectrum of TPQ_{sq} roughly coincides with that of TPQ_{sq} formed in the WT enzyme (see Figure 3B) in the spectral shape and λ_{max} values, unlike those of TPQ_{ox} and TPQ_{ssb}, whose electronic state is affected by the nearby presence of the negatively charged residue Asp298, as described above for the UV/vis absorption spectrum of TPQ_{ox}. The rate of disappearance of TPQ_{ssb} ($k_{+2'}$ = 4.8 × 10^{-4} s^{-1}) is very small and in the same order of magnitude with the steady-state k_{cat} value (1.2 × 10^{-4} s^{-1}) determined at 15 °C for the overall catalytic reaction, suggesting that the step of $TPQ_{ssb} \rightarrow TPQ_{psb}$, which includes the release of α-H^+, is probably rate-limiting in the reductive half-reaction of D298A, and it is therefore concluded that Asp298 plays the most important role in this step. It is noteworthy that the intramolecular electron-transfer step, $TPQ_{red} \rightarrow TPQ_{sq}$, is also considerably slower in the D298A reaction than in the WT reaction. Collectively, Asp298 participates not only directly in the αH^+-abstraction step ($TPQ_{ssb} \rightarrow TPQ_{psb}$) but also indirectly in other steps, including those of $TPQ_{ox} \rightarrow TPQ_{ssb}$ and $TPQ_{red} \rightarrow TPQ_{sq}$. Furthermore, the equilibrium between the TPQ_{red}/Cu^{2+} and TPQ_{sq}/Cu^{1+} couples shifts toward the latter in the WT reaction (k_{+4}/k_{-4} = ∼3.3), whereas it shifts toward the former in the D298A reaction (k_{+4}/k_{-4} = ∼0.3).

X-ray Crystal Structures of the D298A Mutant and Catalytic Intermediates. The D298A mutant enzyme showing

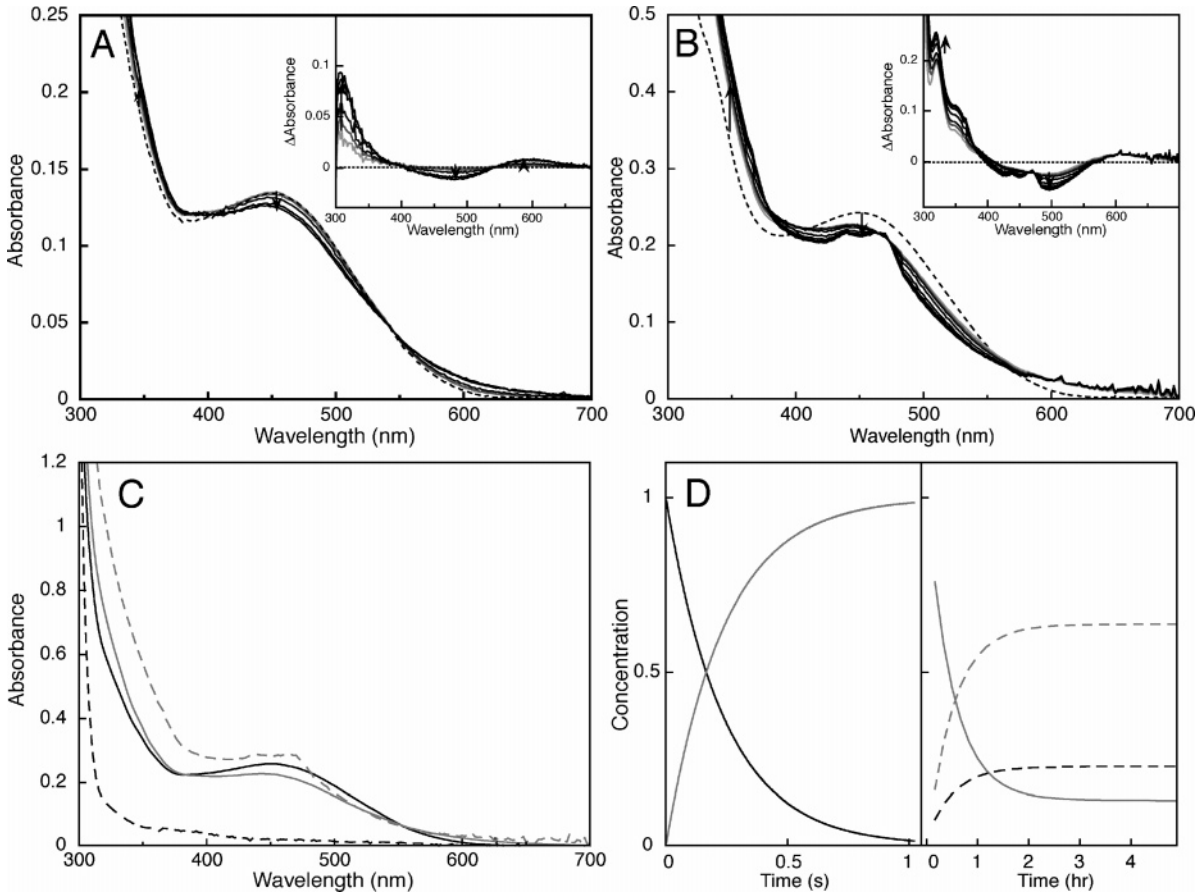

FIGURE 4: Spectral changes during the reductive half-reaction of the D298A mutant of AGAO. (A) UV/vis absorption spectra obtained at 50, 100, 200, 500, and 750 ms (darker spectra represent later times) after mixing the D298A mutant enzyme (0.079 mM subunit) with 0.5 mM 2-PEA in 50 mM HEPES buffer at pH 6.8 and 15 °C using a stopped-flow spectrophotometer are shown. (B) UV/vis absorption spectra obtained at 10, 20, 30, 60, 120, 180, 240, and 300 min (darker spectra represent later times) after manually mixing the D298A mutant (0.14 mM subunit) with 0.5 mM 2-PEA in 50 mM HEPES buffer at pH 6.8 and 15 °C are shown. In both A and B, the dashed line represents the initial spectrum of TPQ_{ox} and arrows indicate the direction of the spectral change. (Insets) Difference spectra obtained by the subtraction of the initial TPQ_{ox} spectrum. (C) Deconvoluted absorption spectra obtained by global analysis are shown for TPQ_{ox} (black solid line), TPQ_{ssb} (gray solid line), TPQ_{red} (black dashed line), and TPQ_{sq} (gray dashed line). (D) Time course of concentration changes of each intermediate.

a minuscule activity was further utilized for structure determination of reaction intermediates, in particular X-ray crystal structures of TPQ_{ssb} and TPQ_{psb}, formed with a true amine substrate, which have not been reported thusfar; the catalytic reaction of D298A was expected to proceed very slowly and coordinately within the crystals. Thus, the crystals of the D298A mutant of AGAO were soaked with the substrate (3 mM 2-PEA) for short (1 h) and long periods (1 week); these crystals are referred to hereafter as D298A/2-PEA(*h*) and D298A/2-PEA(*w*), respectively. The substrate-soaked crystals were then subjected to single-crystal microspectrophotometric analysis at 100 K before exposure to X-rays for spectral identification of reaction intermediates formed, if any, in the crystals. Because the raw spectra of individual crystals showed different absorption intensities because of the difference in crystal thickness, the spectra were mathematically adjusted to have the same absorbance at about 400 nm, corresponding to the isosbestic point observed for the spectral changes of D298A in solution upon the addition of the substrate (see Figure 4A). The crystals of D298A/2-PEA(*h*) exhibited a UV/vis spectrum distinct from that of the substrate-free D298A crystals (Figure 5A) and resembling that of a reaction intermediate of D298A in solution assigned to TPQ_{ssb} (cf. Figure 4C). This clearly shows that the amine oxidation reaction that proceeded in the crystals and the TPQ_{ssb} intermediate was successfully freeze-trapped after 1 h of crystal soaking with the substrate. On the other hand, the crystals of D298A/2-PEA(*w*) showed a spectrum different from those of the substrate-free D298A and D298A/2-PEA(*h*) crystals (Figure 5B) but rather similar to the TPQ_{psb} intermediate formed in the WT enzyme in solution (cf. Figure 3B). Although TPQ_{psb} has not been observed in the reductive half-reaction of D298A in solution presumably because of the relatively fast hydrolysis step ($TPQ_{psb} \rightarrow TPQ_{red}$) as compared with the adjacent steps as described above, the hydrolysis step may be even slow in crystals likely because of the restricted movement of water molecules within the hydrophobic active site (see below), so that the TPQ_{psb} intermediate accumulates in a long period (1 week) of substrate soaking.

Structures of three AGAO derivatives, the substrate-free D298A mutant and those complexed with the substrate, were determined by X-ray crystallography. The refined structures of free D298A, D298A/2-PEA(*h*), and D298A/2-PEA(*w*) gave *R* factors of 19.1, 17.7, and 20.2% and R_{free} of 20.1, 20.1, and 23.2%, respectively (Table 1). The overall structures of free D298A, D298A/2-PEA(*h*), and D298A/2-PEA(*w*) are essentially the same as that of the WT AGAO (PDB

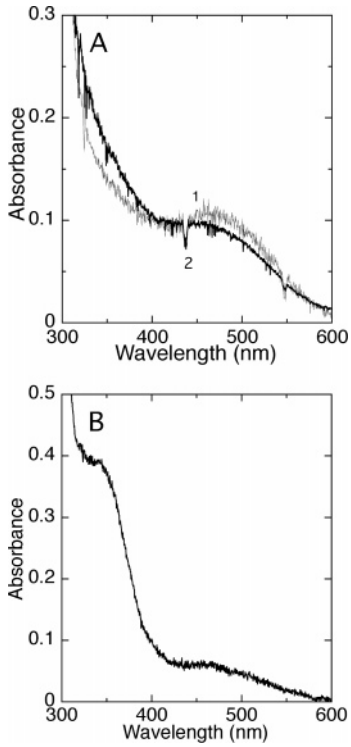

FIGURE 5: UV/vis absorption spectra of D298A crystals. (A) Spectra of D298A crystals (approximate average size, 0.2 × 0.4 × 0.1 mm) before (curve 1) and after (curve 2) soaking with 2-PEA for 1 h. (B) Spectrum of the D298A crystal after soaking with 2-PEA for 1 week.

code 1IU7), with root-mean-square (rms) deviations for 2480 main-chain atoms of 0.48, 0.45, and 0.48 Å, respectively. Electron-density maps clearly showed that the side-chain carboxyl group of Asp298 was missing in all three D298A structures. One of the most obvious differences between the substrate-free D298A and WT structures is the conformation of the TPQ ring (Figure 6A). The TPQ ring in the D298A structure was tilted upward at the C5−C6 edge, with the ring angle of ~21° relative to that of the WT. In addition, the electron density in the $2F_o - F_c$ map was lower around the C5−C6 edge of the TPQ ring than the other part of the ring (data not shown). In reference to this observation, it has been reported for ECAO that the TPQ ring is located in a wedge-shaped pocket and the TPQ ring carbons at the substrate-binding position (C5−C6) have some freedom of movement than other ring carbons at C1−C4 (*19*). The tilting-up of the TPQ ring in the D298A mutant of AGAO might have resulted from the removal of the Asp298 carboxyl group that could anchor the TPQ ring through a weak hydrogen bond to the C5 carbonyl oxygen atom of TPQ, as described earlier. Another conspicuous difference is the orientation of the side chain of Tyr296, rotating by ~104° around its Cα−Cβ bond and invading into the space created by the removal of the Asp298 side chain and tilting-up of the TPQ ring (Figure 6A). Furthermore, a water molecule (Wat1) that is absent in the WT structure is present close to the TPQ O4 in the space evacuated by the conformational change of Tyr296 (Figure 6C). Wat1 is strongly hydrogen-bonding to the TPQ O4 atom (2.6 Å) and the Oϵ atom of the Gln294 side chain (2.7 Å). As described below, Wat1 is maintained also in the TPQ_{ssb} and TPQ_{psb} structures, forming a hydrogen-bonding network in the three D298A structures distinct from the WT structure. These structural differences may lead to differences in electronic features of TPQ described above for the UV/vis and resonance Raman spectra of the WT and D298A mutant enzymes.

The structures of D298A/2-PEA(*h*) and D298A/2-PEA(*w*) have also been refined on the basis of the $2F_o - F_c$ and $F_o - F_c$ maps and also the $F_o - F_c$ omit map. The maps clearly exhibited extra electron densities connected to the C5 position of TPQ even in the initial stage of the structural

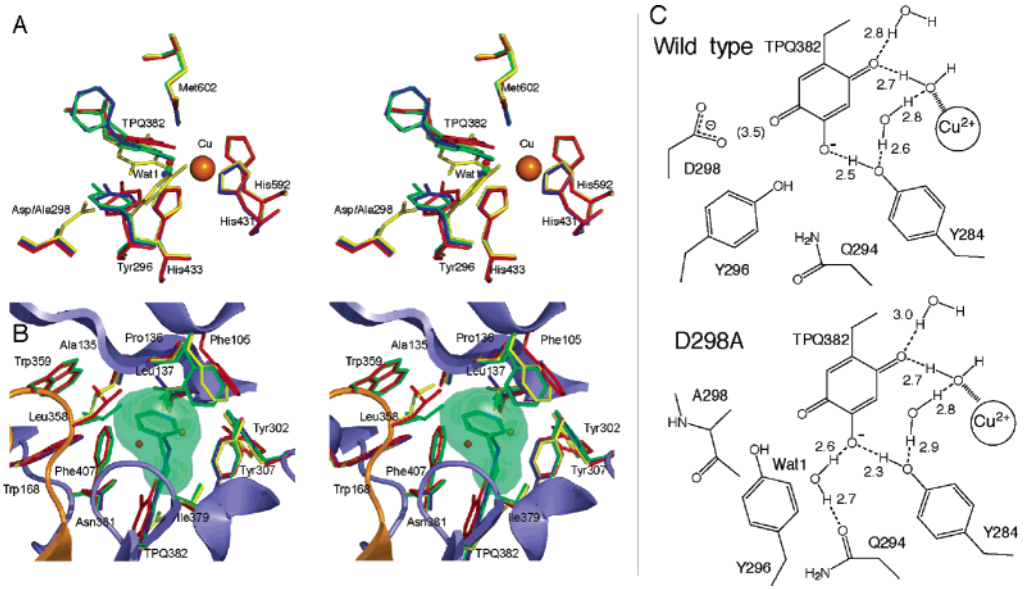

FIGURE 6: Active-site structures of the WT and D298A mutant of AGAO bound with the substrate. (A) Stereodiagram of the superimposed active-site structures: WT (yellow), substrate-free D298A (red), D298A/2-PEA(*h*) (green), and D298A/2-PEA(*w*) (blue) shown in stick representation. Wat1, hydrogen bonding to the TPQ O4 atom, is shown by small spheres. (B) Stereodiagram of the superimposed active-site structures viewed from a direction different from A with parts of main chains shown by ribbons. The pale green region represents the molecular surface of the benzene ring moiety of the bound substrate surrounded by hydrophobic residues. Two water molecules present in the hydrophobic pocket of substrate-free D298A are shown by small spheres. (C) Schematic representation of the active sites of the WT (upper) and D298A mutant (lower) shown with hydrogen-bonding networks. The numbers represent hydrogen-bond distances (Å); those in parentheses are the distances between close but non-hydrogen-bonding atoms.

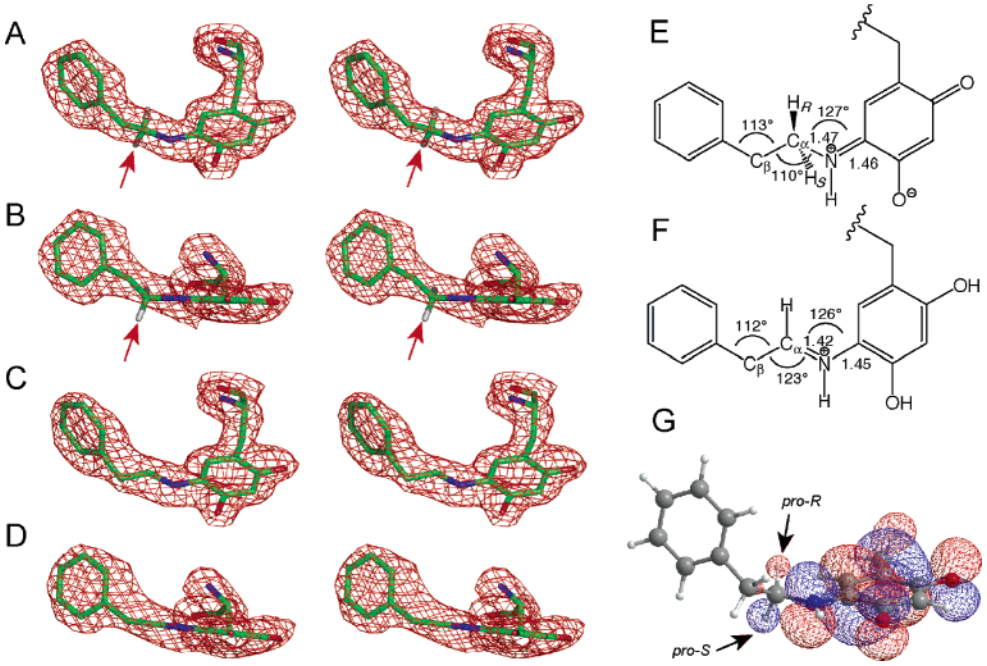

FIGURE 7: Structures of TPQ_{ssb} and TPQ_{psb}. (A) Stereodiagram of the refined model of TPQ_{ssb} shown with an annealed $F_o - F_c$ omit map contoured at 2.8σ. An arrow indicates the computer-generated *pro-S* Cα-hydrogen atom of the substrate. (B) Same as in A but viewed from the direction in parallel with the TPQ ring. (C) Stereodiagram of the refined model of TPQ_{psb} shown with an annealed $F_o - F_c$ omit map contoured at 2.8σ. (D) Same as in C but viewed from the direction in parallel with the TPQ ring. (E) Chemical structure of TPQ_{ssb} shown with bond angles (deg) and lengths (Å) estimated from the crystal structure. (F) Chemical structure of TPQ_{psb} shown with bond angles (deg) and lengths (Å) estimated from the crystal structure. (G) LUMO of the model of TPQ_{ssb}. The coordinates of the side chain of TPQ_{ssb} were taken from the crystal structure of D298A/2-PEA(*h*). The β-carbon atom was changed to a methyl group, and hydrogen atoms were attached as described for the structure E in Scheme 2. Optimization of the structure with fixing the non-hydrogen atoms was carried out with Gaussian 98 at the B3LYP/6-31G(d) level. A single-point calculation was performed at the B3LYP/6-311+G(2d,2p) level, and the molecular orbital was visualized using ChemBats3D (version 9.0.1, CambridgeSoft) at a contour level of ±0.020.

refinement, suggesting the presence of a covalently linked substrate. After the pre-assignments made by single-crystal microspectrophotometry, chemical structures of TPQ_{ssb} and TPQ_{psb} were modeled into the $F_o - F_c$ omit maps obtained for D298A/2-PEA(*h*) and D298A/2-PEA(*w*), respectively. Although the present diffraction data at 1.85-Å resolution were insufficient for judging the bond lengths (i.e., to identify the position of the C═N imine double bond in TPQ_{ssb} and TPQ_{psb}), the omit maps accommodated well the chemical structures of TPQ_{ssb} and TPQ_{psb} (parts A and C of Figure 7, respectively). To further verify the validity of the introduced models, the models were refined in a reverse manner, with the omit maps of D298A/2-PEA(*h*) and D298A/2-PEA(*w*) being calculated using the TPQ_{psb} and TPQ_{ssb} models, respectively. However, the refinements were unsatisfactory in this case; for example, the Cβ atom of TPQ_{psb} was not fitted well within the electron density of D298A/2-PEA(*h*). Moreover, when the shapes of electron densities, particularly the portions extending from the TPQ ring, were compared, that of D298A/2-PEA(*h*) appeared to bent at the position corresponding to the Cα atom of the substrate (Figure 7B), whereas that of D298A/2-PEA(*w*) appeared to bent at the position corresponding to the Cβ atom of the substrate (Figure 7D). In the TPQ_{ssb} and TPQ_{psb} models, in which the Cα atoms have sp^3 and sp^2 configurations, respectively, the Cβ atom of only TPQ_{psb} can be placed in the same plane of the conjugating TPQ ring and the imine double bond (see the N−Cα−Cβ bond angles shown in parts E and F of Figure 7). Hence, the shapes of electron densities also led us to assign the electron densities in the D298A/2-PEA(*h*) and D298A/2-PEA(*w*) structures to TPQ_{ssb} and TPQ_{psb}, respectively. Altogether, we conclude that the structures of D298A/2-PEA(*h*) and D298A/2-PEA(*w*) represent the TPQ_{ssb} and TPQ_{psb} intermediates, respectively. This assignment is also consistent with the soaking period (i.e., forming first TPQ_{ssb} and then TPQ_{psb}, according to the reaction sequence). Although the crystal structures of CAOs complexed with inhibitors have been reported previously (*17*, *44*, *45*), those of catalytic intermediates, TPQ_{ssb} and TPQ_{psb} formed in the crystals by the use of a true amine substrate, have been determined for the first time in the present studies.

As shown in Figure 6A, the active-site structures of D298A/2-PEA(*h*) and D298A/2-PEA(*w*), except for the substrate moieties, are essentially identical with the substrate-free D298A structure, including the side-chain flipping of Tyr296 and the presence of Wat1. The distal part of the substrate (benzene ring) in TPQ_{ssb} and TPQ_{psb} is bound in a hydrophobic pocket constituted by the side chains of Phe105, Ala135, Pro136, Leu137, Trp168, Tyr302, Tyr307, Ile379, Phe407, Leu358, and Trp359 (Figure 6B), among which the last two residues are provided from a large loop (Arm I) (*7*) of the other subunit of the dimer. In the substrate-free WT and D298A structures, six and two water molecules are contained in this pocket, respectively, while no water is contained in the TPQ_{ssb} and TPQ_{psb} structures, with the substrate benzene ring replacing them. Most of the residues constituting the hydrophobic pocket kept the same conformation before and after the substrate binding, but the side chains of Leu358, Tyr302, and Phe105 slightly moved toward the direction of closing the pocket, likely attaining the tight binding of the substrate benzene ring (Figure 6B).

Although hydrogen atoms are invisible at the present 1.8-Å resolution, their coordinates, particularly those connected to carbon atoms, can be automatically generated by a computer. The two prochiral α-hydrogen atoms of the substrate were thus generated in the final model of TPQ_{ssb} (Figure 7A). It is evident that the *pro-S* hydrogen is positioned more perpendicularly to the plane of the Schiff-base/TPQ ring π-electron system than the *pro-R* hydrogen and also is oriented toward Ala298 (Asp298 in the WT enzyme). This orientation of the *pro-S* hydrogen is fully consistent with the stereospecificity of the α-proton abstraction described above.

DISCUSSION

Proposed Mechanism of the Reductive Half-Reaction. On the basis of the results obtained thus far and also the comprehensive description for the catalytic mechanism of CAOs presented by Mure et al. (*15*), a detailed mechanism of the reductive half-reaction of AGAO is proposed as shown in Scheme 2. As inferred from the effect of pH on the steady-state kinetic parameters, the amino group of the substrate [pK_a of 2-PEA = 9.78 (*40*)] is protonated at neutral pH and the positively charged substrate is thereby facilitated to enter the active site through the negatively charged, funnel-shaped channel (*7*, *46*) (step A → B). In the Michaelis complex (B), the substrate amino group must be deprotonated to attack the C5═O carbonyl group of TPQ_{ox} as a nucleophile (*15*) (step B → C). On the other hand, the carboxyl group of Asp298 that should be deprotonated before substrate binding may be protonated in this stage, likely accepting a proton from the substrate amino group (*24*). To undergo facile protonation at neutral pH, the conserved Asp residue commonly possesses an unusually high pK_a value [7.5 for Asp298 of AGAO (this study), 8.1 for Asp319 of HPAO (*39*), and 8.0 for Asp385 of BSAO (*13*, *23*)], which is most likely attained by charge repulsion with the C4 oxoanion of TPQ_{ox} (*15*) (see below) together with the hydrophobic environment of the active site (*47*). The protonated carboxylate of Asp298 would then serve as a general acid, providing a proton back to the hydroxyl group of the carbinolamine intermediate (C) to assist dehydration (steps C → D → E). Consistent with the participation of Asp298 in these initial steps (particularly in the dehydration step), the observed rate of TPQ_{ssb} formation in the D298A mutant enzyme (k_{+1} = 4.7 s^{-1}, Table 4) is about 150-fold smaller than that (699 s^{-1}) of the WT enzyme. This also explains the very low reactivity of the D298A mutant toward phenylhydrazine ($k_{obs}^{WT}/k_{obs}^{D298A}$ = ∼170, Table 2); the reaction with phenylhydrazine also involves a dehydration step prior to the hydrazone formation (*48*). The hydrazino amino group of phenylhydrazine has a pK_a of 5.25 (*49*), and therefore, its deprotonation at neutral pH needs little assistance by Asp298, supporting the greater contribution of Asp298 to the dehydration from the carbinolamine (steps C → D → E) than to the initial deprotonation of the substrate amino group (step A → B). Hence, the first intermediate observed by the pre-steady-state kinetic analysis is TPQ_{ssb}, with the substrate amino nitrogen atom attached to the C5 carbon of TPQ in an imine double bond, and the carboxylate of Asp298 is deprotonated again (E). The twitter ionic structure of TPQ_{ssb} is stabilized by a strong electrostatic interaction of the C4 oxoanion of TPQ with the protonated imine nitrogen of the neighboring Schiff base (*16*).

Although the exact pK_a values of the α hydrogen of amines are not known, the value would not be so much different from the value of the hydrogen of tetramethylammonium [pK_a = 42 (*50*)] and would be much higher than 20. Therefore, because it is almost undissociable in the physiological pH region, the Schiff-base formation with the substrate amino group is regarded to be a very important function of the TPQ cofactor, lowering the pK_a of the α-hydrogen atom to a dissociable level. Such a function is also common to pyridoxal 5′-phosphate (PLP) that was erroneously believed to be the elusive cofactor of CAOs until the early 1980's (*51*). In the initial step of the PLP-dependent enzyme reactions with the α-amino acid as a general substrate, the α-hydrogen atom of amino acids, which has pK_a values of >20 (*52*), must be removed by the ϵ-amino group of the Lys residue involved in the binding of PLP, which has a pK_a value of ∼10.5. In aspartate aminotransferase, the pK_a value of the substrate α-hydrogen atom is estimated to be decreased to around 13, as calculated from the equilibrium constant (∼10^2) (*53*) between the substrate−PLP Schiff base (Lys unprotonated) and its deprotonated structure (Lys protonated). Similarly, the pK_a of the α-hydrogen atom of the amine substrate in TPQ_{ssb} should be sufficiently lowered enough to be released slowly even without the proton-abstracting base in the D298A mutant.

Once TPQ_{ssb} is formed, the carboxyl group of Asp298 with a decreased pK_a of ∼6.5 (see above) would then act as a general base, effectively abstracting a proton from TPQ_{ssb} (step E → F). Although this step is not rate-limiting in the reductive half-reaction of WT AGAO ($k_{+2} > k_{+3}$, Table 4), the α-proton abstraction from TPQ_{ssb} is the most important catalytic role of Asp298, as manifested in the largest drop of the rate constant for this step by the Asp298-to-Ala mutation ($k_{+2}^{WT}/k_{+2'}^{D298A}$ = ∼10^6). Concomitant with the stereospecific abstraction of the *pro-S* α-H^+ of the substrate in the TPQ_{ssb} intermediate by the deprotonated carboxylate of Asp298, the C2═O oxygen atom of TPQ may accept a proton from a water molecule that is hydrogen-bonding to it (step E → F). This water is stabilized by coordination to the bound Cu^{2+} ion and would easily donate a proton (pK_a = 7.5) (*54*). The resultant TPQ_{psb} is formally a $2e^-$-reduced form of TPQ, in which electrons are derived from the substrate amine. Although the C4 hydroxyl group of TPQ_{ox} has a very low pK_a [4.1 in a model compound (*38*) and ∼3 in BSAO (*38*) and AGAO (*55*)], the same group in TPQ_{psb} is likely to have a high pK_a of about 9 because of the reduced TPQ ring (F) (*38*). Thus, the C4 oxoanion easily accepts a proton from the protonated carboxyl group of Asp298 (step F → G), which originates from the substrate Cα position. Protonation of the C4 oxygen then leads to the reduced stability of TPQ_{psb} that arises from a loss of electrostatic stabilization between the C4 oxoanion and the Schiff-base imine nitrogen (G) (*15*). Although TPQ_{psb} was not observed in the reaction of D298A, likely because of a faster rate of disappearance than that of formation and, therefore, the rate constant for TPQ_{psb} hydrolysis could not be compared between the WT and D298A reactions, Asp298 may also participate in the hydrolysis of TPQ_{psb} by raising the basicity of the water molecule attacking the imine carbon atom (step H → I). Finally, the aminoresorcinol form of TPQ_{red} (J) is

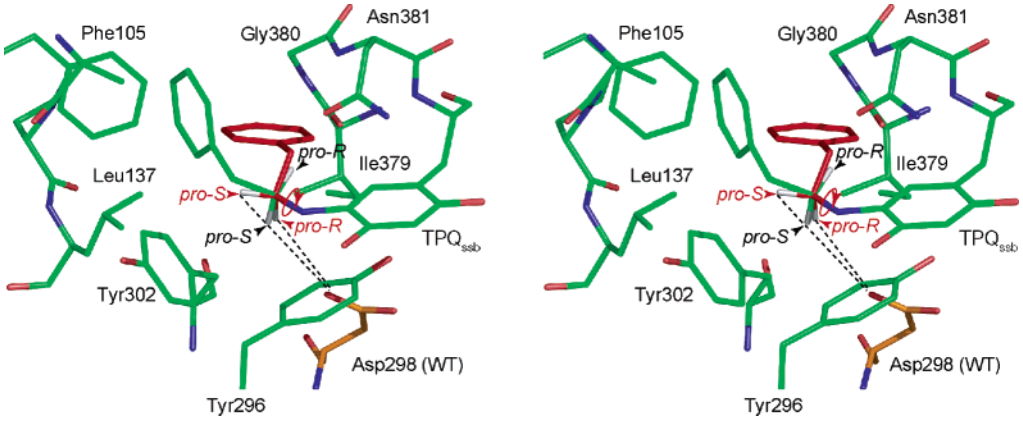

FIGURE 8: Modeling of an alternative conformation of TPQ_{ssb}. An alternative conformation of TPQ_{ssb} was manually modeled by rotating around the N−Cα bond of TPQ_{ssb} obtained in the X-ray crystal structure, so that the *pro-R* α-hydrogen atom is positioned perpendicularly to the Schiff-base/TPQ plane. Stereodiagram of active-site residues of the D298A mutant is shown in a stick representation (red). Asp298 of the WT enzyme is also shown (orange). The two prochiral hydrogen atoms (*pro-S* and *pro-R*) in the two conformations are indicated by arrows.

formed concomitantly with the release of the product aldehyde (steps I → J → K). The Cu^{2+}-coordinating hydroxide ion may be reprotonated indirectly by the protonated carboxyl group of Asp298 through the hydrogen-bonding network conserved in the active site (see Figure 6C).

In the single-turnover reductive half-reaction of AGAO under anaerobic conditions, the spectroscopically observed final form of TPQ is TPQ_{sq} (Figure 3A), resulting from a single electron transfer from TPQ_{red} to the bound Cu^{2+} ion (step K → L). This intramolecular electron-transfer step, $TPQ_{red} \rightarrow TPQ_{sq}$, is the slowest step, with a rate constant (k_{+4}) being only twice the overall k_{cat} value, (Table 4) and hence appears to be off the overall reaction cycle, as reported previously (*8*, *22*). However, TPQ_{sq} has been proposed to be a kinetically competent intermediate in the catalysis of CAOs, on the basis of the observation for the temperature-dependent, rapid equilibrium between Cu^{2+}/TPQ_{red} and Cu^{1+}/TPQ_{sq} (*20*, *21*). In relation to this argument, we have recently determined the crystal structure of AGAO anaerobically reduced with the substrate and found that TPQ_{red} (or TPQ_{sq}) is in a catalytically inactive "on-copper" conformation (*7*) with the C4−O^- atom of TPQ positioned at a distance of 2.7 Å from the bound copper ion (Okajima, T., unpublished data) (see Scheme 2, L). Thus, it is likely that the slow step of $TPQ_{red} \rightarrow TPQ_{sq}$ (k_{+4}) determined from the pre-steady-state kinetics reflects the conformational change of TPQ_{red} from the catalytically active "off-copper" conformation to the inactive on-copper one, in which the intramolecular electron transfer from TPQ_{red} to Cu^{2+} would certainly occur very rapidly.

Implications for Stereospecificity of α*-Proton Abstraction.* The stereospecificity of proton abstraction from the Cα position of the substrate has been studied for CAOs from various organisms (*17*, *56*, *57*). Interestingly, the stereospecificity is variable depending upon the enzyme sources and substrate amines used. For example, the *pro-S* proton of dopamine is abstracted in the reaction of PSAO, while the *pro-R* proton of the same amine is abstracted in the reaction of porcine plasma enzyme (*57*). On the other hand, BSAO is nonstereospecific for dopamine but is *pro-S*-specific for another substrate, benzylamine (*56*, *57*). We have recently shown that AGAO stereospecifically abstracts the *pro-S* α-H^+ of 2-PEA (*25*), similar to plant and other bacterial CAOs (*17*, *57*). In view of the highly conserved active-site structures of this enzyme family (*7*−*14*), the origin of the inconsistent stereospecificity remains to be settled. The wider and deeper funnel-shaped substrate channel of BSAO than that of other CAOs (*13*) may correlate with its broad substrate specificity and the stereochemical ambiguity. For AGAO, it is very important to note that the *pro-S* stereospecificity is maintained even in the absence of the catalytic base (Asp298), as described above. This observation strongly suggests that the stereospecificity of α-H^+ abstraction is not simply determined by the relative geometry of TPQ and the α-proton-abstracting catalytic base.

To gain further insight into the stereospecificity of α-proton abstraction, the two prochiral α-hydrogen atoms were generated in the final model of TPQ_{ssb} (Figure 7A). Consistent with the stereospecificity of AGAO, the *pro-S* hydrogen indeed directs toward Ala298 (Asp298 in the WT enzyme) and is located closer to Ala298 than the *pro-R* hydrogen. More importantly, however, in this conformation of TPQ_{ssb}, the *pro-S* hydrogen is positioned nearly perpendicularly to the plane of the Schiff base/TPQ ring, so that the σ orbital of the Cα−H_S bond maximally overlaps with the π orbital of TPQ_{ssb}. Preferential σ-bond cleavage by such maximal orbital overlap was originally hypothesized by Dunathan for PLP-dependent enzyme reactions, in which one of the three σ bonds cleaved around the Cα atom of the amino acid substrate should be oriented perpendicularly to the Schiff-base/PLP plane (*58*). Furthermore, when the molecular orbitals of TPQ_{ssb} were calculated by a DFT method (B3LYP) using Gaussian 98 (*59*) and the coordinates of TPQ_{ssb} were obtained in this study, LUMO of the *pro-S* hydrogen atom was found to be more widely and densely protruding into the space than that of the *pro-R* hydrogen atom (Figure 7G), suggesting that the LUMO of the *pro-S* hydrogen is highly advantageous for the interaction with the HOMO of a proton acceptor, the deprotonated carboxylate oxygen atom of Asp298 in the WT enzyme or an oxygen atom of a nearby water molecule in the D298A mutant. Altogether, these results lead to a new proposal that the stereospecificity of α-proton abstraction is primarily determined by the conformation of TPQ_{ssb}, rather than the relative geometry of TPQ and the catalytic base.

If the stereospecificity of α-proton abstraction is indeed determined by the conformation of TPQ_{ssb}, the active-site structure of each CAO, particularly the local region that binds a distal part of the amine substrate (the opposite end of the amino group), should be taken into account, because the conformation of TPQ_{ssb} is allowed to vary by the rotation around the N−Cα and Cα−Cβ bonds (see Figure 7E) but is fixed upon binding of the distal part of substrate (benzene ring in the case of 2-PEA) to the enzyme active site. Residues constituting the hydrophobic pocket for binding of the benzene ring of 2-PEA in AGAO (Figure 6B) are only poorly conserved. Thus, it is strongly suggested that the inconsistent stereospecificity of α-proton abstraction among various CAOs arises from the difference in the structures of the substrate-binding pocket that ultimately controls the conformation of TPQ_{ssb}. To examine this hypothesis, the conformation of TPQ_{ssb} has been manually modeled in the active site of AGAO, so that the *pro-R* α-hydrogen atom is positioned perpendicularly to the Schiff-base/TPQ plane by rotating around the N−Cα bond (Figure 8). In this conformation, the distance to the carboxyl group of Asp298 (modeled into the D298A structure) is also 1.7-Å shorter for the *pro-R* hydrogen atom than for the *pro-S* hydrogen. However, significant steric hindrances are evoked between the active-site residues and the benzene ring or other parts of the substrate, for example, the C6 H atom of the TPQ ring versus the Cβ atom of 2-PEA and the side-chain methyl group of Ile379 versus the benzene ring H atoms of 2-PEA. Therefore, this conformation of TPQ_{ssb} with the perpendicularly positioned *pro-R* hydrogen atom is not allowed in practice for AGAO with 2-PEA as the substrate. Nevertheless, a smaller amine such as ethylamine may be able to take alternative conformations of TPQ_{ssb}. Indeed, a preliminary experiment with stereospecifically [^{2}H]-labeled ethylamine as the substrate has shown a notable decrease (to as low as 88%) of the *pro-S* stereospecificity for α-proton abstraction by AGAO (Yamamoto, Y., unpublished data).

In conclusion, the present study unequivocally demonstrates that Asp298 of AGAO, corresponding to the Asp residue strictly conserved in the active site of CAOs, functions as a general acid/base catalyst participating not only in the α-proton abstracting step but also in other steps involving proton transfer during the reductive half-reaction of the catalytic cycle. More intriguingly, the stereospecificity for α-proton abstraction is inherently determined by the conformation of the TPQ_{ssb} intermediate, rather than the relative geometry of TPQ and the catalytic base.

REFERENCES

1. McIntire, W. S., and Hartmann, C. (1993) Copper-containing amine oxidases, in *Principles and Applications of Quinoproteins* (Davidson, V. L., Ed.) pp 97−171, Marcel Dekker, New York.
2. Klinman, J. P., and Mu, D. (1994) Quinoenzymes in biology, *Annu. Rev. Biochem. 63*, 299−344.
3. Knowles, P. F., and Dooley, D. M. (1994) Amine oxidases, in *Metal Ions in Biological Systems* (Sigel, H., and Sigel, A., Eds.) Vol. 30, pp 361−403, Marcel Dekker, New York.
4. Matsuzaki, R., Fukui, T., Sato, H., Ozaki, Y., and Tanizawa, K. (1994) Generation of the topa quinone cofactor in bacterial monoamine oxidase by cupric ion-dependent autooxidation of a specific tyrosyl residue, *FEBS Lett. 351*, 360−364.
5. Cai, D., and Klinman, J. P. (1994) Copper amine oxidase: Heterologous expression, purification, and characterization of an active enzyme in *Saccharomyces cerevisiae*, *Biochemistry 33*, 7647−7653.
6. Choi, Y. H., Matsuzaki, R., Fukui, T., Shimizu, E., Yorifuji, T., Sato, H., Ozaki, Y., and Tanizawa, K. (1995) Copper/topa quinone-containing histamine oxidase from *Arthrobacter globiformis*. Molecular cloning and sequencing, overproduction of precursor enzyme, and generation of topa quinone cofactor, *J. Biol. Chem. 270*, 4712−4720.
7. Wilce, M. C. J., Dooley, D. M., Freeman, H. C., Guss, J. M., Matsunami, H., McIntire, W. S., Tanizawa, K., and Yamaguchi, H. (1997) Crystal structures of the copper-containing amine oxidase from *Arthrobacter globiformis* in the holo and apo forms: Implications for the biogenesis of topaquinone, *Biochemistry 36*, 16116−16133.
8. Kishishita, S., Okajima, T., Kim, M., Yamaguchi, H., Hirota, S., Suzuki, S.,Kuroda, S., Tanizawa, K., and Mure, M. (2003) Role of copper ion in bacterial copper amine oxidase: Spectroscopic and crystallographic studies of metal-substituted enzymes, *J. Am. Chem. Soc. 125*, 1041−1055.
9. Kumar, V., Dooley, D. M., Freeman, H. C., Guss, J. M., Harvey, I., McGuirl, M. A., Wilce, M. C., and Zubak, V. M. (1996) Crystal structure of a eukaryotic (pea seedling) copper-containing amine oxidase at 2.2 Å resolution, *Structure 4*, 943−955.
10. Parsons, M. R., Convery, M. A., Wilmot, C. M., Yadav, K. D., Blakeley, V., Corner, A. S., Phillips, S. E., McPherson, M. J., and Knowles, P. F. (1995) Crystal structure of a quinoenzyme: Copper amine oxidase of *Escherichia coli* at 2 Å resolution, *Structure 3*, 1171−1184.
11. Li, R., Klinman, J. P., and Mathews, F. S. (1998) Copper amine oxidase from *Hansenula polymorpha*: The crystal structure determined at 2.4 Å resolution reveals the active conformation, *Structure 6*, 293−307.
12. Duff, A. P., Cohen, A. E., Ellis, P. J., Kuchar, J. A., Langley, D. B., Shepard, E. M., Dooley, D. M., Freeman, H. C., and Guss, J. M. (2003) The crystal structure of *Pichia pastoris* lysyl oxidase, *Biochemistry 42*, 15148−15157.
13. Lunelli, M., Di Paolo, M. L., Biadene, M., Calderone, V., Battistutta, R., Scarpa, M., Rigo, A., and Zanotti, G. (2005) Crystal structure of amine oxidase from bovine serum, *J. Mol. Biol. 346*, 991−1004.
14. Airenne, T. T., Nymalm, Y., Kidron, H., Smith, D. J., Pihlavisto, M., Salmi, M., Jalkanen, S., Johnson, M. S., and Salminen, T. A. (2005) Crystal structure of the human vascular adhesion protein-1: Unique structural features with functional implications, *Protein Sci. 14*, 1964−1974.
15. Mure, M., Mills, S. A., and Klinman, J. P. (2002) Catalytic mechanism of the topa quinone containing copper amine oxidases, *Biochemistry 41*, 9269−9278.
16. Mure, M., and Klinman, J. P. (1995) Model studies of topaquinone-dependent amine oxidases. 2. Characterization of reaction intermediates and mechanism, *J. Am. Chem. Soc. 117*, 8707−8718.
17. Wilmot, C. M., Murray, J. M., Alton, G., Parsons, M. R., Convery, M. A., Blakeley, V., Corner, A. S., Palcic, M. M., Knowles, P. F., McPherson, M. J., and Phillips, S. E. (1997) Catalytic mechanism of the quinoenzyme amine oxidase from *Escherichia coli*: Exploring the reductive half-reaction, *Biochemistry 36*, 1608−1620.
18. Plastino, J., Green, E. L., Sanders-Loehr, J., and Klinman, J. P. (1999) An unexpected role for the active site base in cofactor orientation and flexibility in the copper amine oxidase from *Hansenula polymorpha*, *Biochemistry 38*, 8204−8216.
19. Murray, J. M., Saysell, C. G., Wilmot, C. M., Tambyrajah, W. S., Jaeger, J., Knowles, P. F., Phillips, S. E., and McPherson, M. J. (1999) The active site base controls cofactor reactivity in *Escherichia coli* amine oxidase: X-ray crystallographic studies with mutational variants, *Biochemistry 38*, 8217−8227.
20. Dooley, D. M., McGuirl, M. A., Brown, D. E., Turowski, P. N., McIntire, W. S., and Knowles, P. F. (1991) A Cu(I)-semiquinone state in substrate-reduced amine oxidases, *Nature 349*, 262−264.
21. Turowski, P. N., McGuirl, M. A., and Dooley, D. M. (1993) Intramolecular electron-transfer rate between active-site copper and topa quinone in pea seedling amine oxidase, *J. Biol. Chem. 268*, 17680−17682.
22. Su, Q., and Klinman, J. P. (1998) Probing the mechanism of proton coupled electron transfer to dioxygen: The oxidative half-reaction of bovine serum amine oxidase, *Biochemistry 37*, 12513−12525.
23. Farnum, M., Palcic, M., and Klinman, J. P. (1986) pH dependence of deuterium isotope effects and tritium exchange in the bovine plasma amine oxidase reaction: A role for single-base catalysis in amine oxidation and imine exchange, *Biochemistry 25*, 1898−1904.

24. Saysell, C. G., Tambyrajah, W. S., Murray, J. M., Wilmot, C. M., Phillips, S. E., McPherson, M. J., and Knowles, P. F. (2002) Probing the catalytic mechanism of *Escherichia coli* amine oxidase using mutational variants and a reversible inhibitor as a substrate analogue, *Biochem. J. 365*, 809−816.
25. Uchida, M., Ohtani, A., Kohyama, N., Okajima, T., Tanizawa, K., and Yamamoto, Y. (2003) Stereochemistry of 2-phenylethylamine oxidation catalyzed by bacterial copper amine oxidase, *Biosci., Biotechnol., Biochem. 67*, 2664−2667.
26. Ruggiero, C. E., and Dooley, D. M. (1999) Stoichiometry of the topa quinone biogenesis reaction in copper amine oxidases, *Biochemistry 38*, 2892−2898.
27. Ellis, K. J., and Morrison, J. F. (1982) Buffers of constant ionic strength for studying pH-dependent processes, *Methods Enzymol. 87*, 405−426.
28. Cleland, W. W. (1979) Statistical analysis of enzyme kinetic data, *Methods Enzymol. 63*, 103−138.
29. Leslie, A. G. W. (1992) *Joint CCP4 and EESF-EACMB Newsletter on Protein Crystallography*, SERC Daresbury Laboratory, Warrington, U.K.
30. Collaborative Computational Project Number 4 (1994) The CCP 4 suite: Programs for protein crystallography, *Acta Crystallogr., Sect. D: Biol. Crystallogr. 50*, 760−763.
31. Brünger, A. T., Adams, P. D., Clore, G. M., DeLano, W. L., Gros, P., Grosse-Kunstleve, R. W., Jiang, J. S., Kuszewski, J., Nilges, M., Pannu, N. S., Read, R. J., Rice, L. M., Simonson, T., and Warren, G. L. (1998) Crystallography and NMR system: A new software suite for macromolecular structure determination, *Acta Crystallogr., Sect. D: Biol. Crystallogr. 54*, 905−921.
32. McRee, D. E. (1999) XtalView/Xfit−A versatile program for manipulating atomic coordinates and electron density, *J. Struct. Biol. 125*, 156−165.
33. Kleywegt, G. J., and Jones, T. A. (1997) Model building and refinement practice, *Methods Enzymol. 277*, 208−230.
34. Janes, S. M., and Klinman, J. P. (1991) An investigation of bovine serum amine oxidase active site stoichiometry: Evidence for an aminotransferase mechanism involving two carbonyl cofactors per enzyme dimmer, *Biochemistry 30*, 4599−4605.
35. Okajima, T., Kishishita, S., Chiu, Y.-C., Murakawa, T., Kim, M., Yamaguchi, H., Hirota, S., Kuroda, S., and Tanizawa, K. (2005) Reinvestigation of metal ion specificity for quinone cofactor biogenesis in bacterial copper amine oxidase, *Biochemistry 44*, 12041−12048.
36. Paz, M. A., Flückiger, R., Boak, A., Kagan, H. M., and Gallop, P. M. (1991) Specific detection of quinoproteins by redox-cycling staining, *J. Biol. Chem. 266*, 689−692.
37. Nakamura, N., Moenne-Loccoz, P., Tanizawa, K., Mure, M., Suzuki, S., Klinman, J. P., and Sanders-Loehr, J. (1997) Topaquinone-dependent amine oxidases: Identification of reaction intermediates by Raman spectroscopy, *Biochemistry 36*, 11479−11486.
38. Mure, M., and Klinman, J. P. (1993) Synthesis and spectroscopic characterization of model compounds for the active site cofactor in copper amine oxidases, *J. Am. Chem. Soc. 115*, 7117−7127.
39. Hevel, J. M., Mills, S. A., and Klinman, J. P. (1999) Mutation of a strictly conserved, active-site residue alters substrate specificity and cofactor biogenesis in a copper amine oxidase, *Biochemistry 38*, 3683−3693.
40. Tuckerman, M. M., Mayer, J. R., and Nachod, F. C. (1959) Anomalous pK_a values of some substituted phenylethylamines, *J. Am. Chem. Soc. 81*, 92−94.
41. Steinebach, V., de Vries, S., and Duine, J. A. (1996) Intermediates in the catalytic cycle of copper-quinoprotein amine oxidase from *Escherichia coli*, *J. Biol. Chem. 271*, 5580−5588.
42. Hartmann, C., Brzovic, P., and Klinman, J. P. (1993) Spectroscopic detection of chemical intermediates in the reaction of para-substituted benzylamines with bovine serum amine oxidase, *Biochemistry 32*, 2234−2241.
43. Hirota, S., Iwamoto, T., Kishishita, S., Okajima, T., Yamaguchi, O., and Tanizawa, K. (2001) Spectroscopic observation of intermediates formed during the oxidative half-reaction of copper/topa quinone-containing phenylethylamine oxidase, *Biochemistry 40*, 15789−15796.
44. O'Connell, K. M., Langley, D. B., Shepard, E. M., Duff, A. P., Jeon, H.-B., Sun, G., Freeman, H. C., Guss, J. M., Sayre, L. M., and Dooley, D. M. (2004) Differential inhibition of six copper amine oxidases by a family of 4-(aryloxy)-2-butynamines: Evidence for a new mode of inactivation, *Biochemistry 43*, 10965−10978.
45. Mure, M., Brown, D. E., Saysell, C., Rogers, M. S., Wilmot, C. M., Kurtis, C. R., McPherson, M. J., Phillips, S. E., Knowles, P. F., and Dooley, D. M. (2005) Role of the interactions between the active site base and the substrate Schiff base in amine oxidase catalysis. Evidence from structural and spectroscopic studies of the 2-hydrazinopyridine adduct of *Escherichia coli* amine oxidase, *Biochemistry 44*, 1568−1582.
46. Matsuzaki, R., and Tanizawa, K. (1998) Exploring a channel to the active site of copper/topaquinone-containing phenylethylamine oxidase by chemical modification and site-specific mutagenesis, *Biochemistry 37*, 13947−13957.
47. Fersht, A. (1998) *Structure and Mechanism in Protein Science*, W. H. Freeman and Company, New York.
48. Medda, R., Padiglia, A., Pedersen, J. Z., Rotilio, G., Finazzi Agrò, A., and Floris, G. (1995) The reaction mechanism of copper amine oxidase: Detection of intermediates by the use of substrates and inhibitors, *Biochemistry 34*, 16375−16381.
49. do Amaral, L., Sandstron, W. A., and Cordes, E. H. (1966) Some aspects of mechanism and catalysis for carbonyl addition reactions, *J. Am. Chem. Soc. 88*, 2225−2233.
50. Zhang, X. M., and Bordwell, F. G. (1994) Equilibrium acidities and homolytic bond-dissociation energies of the acidic C−H bonds in P-substituted triphenylphosphonium cations, *J. Am. Chem. Soc. 116*, 968−972.
51. Agro, A. F., Guerrieri, P., Costa, M. T., and Mondovi, B. (1977) On the nature of chromophore in pig kidney diamine oxidase, *Eur. J. Biochem. 74*, 435−440.
52. Rios, A., Amyes, T. L., and Richard, J. P. (2000) Formation and stability of organic zwitterions in aqueous solution: Enolates of the amino acid glycine and its derivatives, *J. Am. Chem. Soc. 122*, 9373−9385.
53. Hayashi, H., and Kagamiyama, H. (1995) Reaction of aspartate aminotransferase with L-erythro-3-hydroxyaspartate: Involvement of Tyr70 in stabilization of the catalytic intermediates, *Biochemistry 34*, 9413−9423.
54. Kyte, J. (1995) *Mechanism in Protein Chemistry*, Garland Publishing, Inc., New York.
55. Kishishita, S. (1997) M.S. Thesis, Osaka University, Osaka, Japan.
56. Battersby, A. R., Staunton, J., Klinman, J., and Summers, M. C. (1979) Stereochemistry of oxidation of benzylamine by the amine oxidase from beef plasma, *FEBS Lett. 99*, 297−298.
57. Coleman, A. A., Hindsgaul, O., and Palcic, M. M. (1989) Stereochemistry of copper amine oxidase reactions, *J. Biol. Chem. 264*, 19500−19505.
58. Dunathan, H. C. (1966) Conformation and reaction specificity in pyridoxal phosphate enzymes, *Proc. Natl. Acad. Sci. U.S.A. 55*, 712−716.
59. Frisch, M. J., Trucks, G. W., Schlegel, H. B., Scuseria, G. E., Robb, M. A., Cheeseman, J. R., Zakrzewski, V. G., Montgomery, J. A., Jr., Stratmann, R. E., Burant, J. C., Dapprich, S., Millam, J. M., Daniels, A. D., Kudin, K. N., Strain, M. C., Farkas, O., Tomasi, J., Barone, V., Cossi, M., Cammi, R., Mennucci, B., Pomelli, C., Adamo, C., Clifford, S., Ochterski, J., Petersson, G. A., Ayala, P. Y., Cui, Q., Morokuma, K., Malick, D. K., Rabuck, A. D., Raghavachari, K., Foresman, J. B., Cioslowski, J., Ortiz, J. V., Baboul, A. G., Stefanov, B. B., Liu, G., Liashenko, A., Piskorz, P., Komaromi, I., Gomperts, R., Martin, R. L., Fox, D. J., Keith, T., Al-Laham, M. A., Peng, C. Y., Nanayakkara, A., Challacombe, M., Gill, P. M. W., Johnson, B., Chen, W., Wong, M. W., Andres, J. L., Gonzalez, C., Head-Gordon, M., Replogle, E. S., and Pople, J. A. (1998) *Gaussian 98, Revision A.9*, Gaussian, Inc., Pittsburgh, PA.

BI052464L